Dystroglycan Maintains Inner Limiting Membrane Integrity to Coordinate Retinal Development

Reena Clements[1], Rolf Turk[3], Kevin P. Campbell[3], and Kevin M. Wright[1,2, #]

1) Neuroscience Graduate Program, 2) Vollum Institute, Oregon Health & Science University, Portland, OR 97239, USA, 3) Howard Hughes Medical Institute, Department of Molecular Physiology and Biophysics, Department of Neurology, Department of Internal Medicine, The University of Iowa Roy J. and Lucille A. Carver College of Medicine, Iowa City, IA 52242, USA.

#) Correspondence to Kevin M Wright (wrighke@ohsu.edu). Vollum Institute, 3181 SW Sam Jackson Park Rd L474 Portland, OR 97239. (503)-494-6955

Abbreviated Title**:** Dystroglycan regulates retinal development

Acknowledgements

We thank Patrick Kerstein and Kylee Rosette for their technical assistance; Marla Feller and Franklin Caval-Holme for advice on visualizing and analyzing retinal waves; W. Rowland Taylor and Teresa Puthussery and members of their labs for antibodies and technical advice; David Pow for the GlyT1 antibody; Catherine Morgans for the mGluR6 antibody, Stefanie Kaech Petrie and the OHSU Advanced Light Microscopy Core (ALM) for assistance with confocal imaging; David Ginty, Alex Kolodkin, Martin Riccomagno, Randall Hand and members of the Campbell and Wright laboratories for discussion throughout the course of this study and comments on the manuscript. This work was supported by NIH Grants R01-NS091027 (K.M.W.), The Whitehall Institute (K.M.W.), The Medical Research Foundation of Oregon (K.M.W.), NSF GRFP (R.C.), LaCroute Neurobiology of Disease Fellowship (R.C.), Tartar Trust Fellowship (R.C.), NINDS P30–NS061800 (OHSU ALM), and a Paul D. Wellstone Muscular Dystrophy Cooperative Research Center grant to K.P.C. (1U54NS053672). K.P.C. is an investigator of the Howard Hughes Medical Institute.

Abstract

Proper neural circuit formation requires the precise regulation of neuronal migration, axon guidance and dendritic arborization. Mutations affecting the function of the transmembrane glycoprotein dystroglycan cause a form of congenital muscular dystrophy that is frequently associated with neurodevelopmental abnormalities. Despite its importance in brain development, the role for dystroglycan in regulating retinal development remains poorly understood. Using a mouse model of dystroglycanopathy (*ISPD*^{L79*}) and conditional *dystroglycan* mutants of both sexes, we show that dystroglycan is critical for the proper migration, axon guidance and dendritic stratification of neurons in the inner retina. Using genetic approaches, we show that dystroglycan functions in neuroepithelial cells as an extracellular scaffold to maintain the integrity of the retinal inner limiting membrane (ILM). Surprisingly, despite the profound disruptions in inner retinal circuit formation, spontaneous retinal activity is preserved. These results highlight the importance of dystroglycan in coordinating multiple aspects of retinal development.

Significance Statement

The extracellular environment plays a critical role in coordinating neuronal migration and neurite outgrowth during neural circuit development. The transmembrane glycoprotein dystroglycan functions as a receptor for multiple extracellular matrix proteins, and its dysfunction leads to a form of muscular dystrophy frequently associated with neurodevelopmental defects. Our results demonstrate that dystroglycan is required for maintaining the structural integrity of the inner limiting membrane (ILM) in

24 the developing retina. In the absence of functional dystroglycan, ILM degeneration leads
25 to defective migration, axon guidance and mosaic spacing of neurons, and a loss of
26 multiple neuron types during retinal development. These results demonstrate that
27 disorganization of retinal circuit development is a likely contributor to visual dysfunction
28 in patients with dystroglycanopathy.
29

30 **Introduction**

31 The precise lamination of neurons is critical for establishing proper connectivity in
32 the developing nervous system. The retina is organized in three cellular layers: the
33 outer nuclear layer (ONL) comprised of rod and cone photoreceptors; the inner nuclear
34 layer (INL) containing horizontal cells, bipolar cells and amacrine cells; and the ganglion
35 cell layer containing RGCs and displaced amacrine cells (Bassett and Wallace, 2012).
36 Two synaptic lamina form postnatally: the outer plexiform layer (OPL), which contains
37 synapses between photoreceptors, bipolar cells and horizontal cells; and the inner
38 plexiform layer (IPL), which contains synapses between bipolar cells, amacrine cells
39 and RGCs. The molecular cues that direct the laminar positioning of neurons and the
40 stratification of their processes within the synaptic layers remain poorly understood.

41 Unlike the cerebral cortex, where many neurons migrate along the radial glia
42 scaffold, retinal migration does not require contact between neurons and neuroepithelial
43 cells (Reese, 2011). RGCs, bipolar cells, and photoreceptors migrate by nuclear
44 translocation through a basally-directed process. Basal process contact with the inner
45 limiting membrane (ILM) is critical for the polarization and migration of RGCs (Randlett
46 et al., 2011). The ILM is enriched with extracellular matrix (ECM) proteins including

47 laminins, Collagen IV, and perlecan (Taylor et al., 2015; Varshney et al., 2015).
48 Mutations in specific laminins (Lamα1, Lamβ2 and Lamγ3) or the laminin receptor β1-
49 Integrin disrupt formation of the ILM and organization of the ganglion cell layer (GCL)
50 (Edwards et al., 2010; Pinzon-Duarte et al., 2010; Gnanaguru et al., 2013; Riccomagno
51 et al., 2014). How laminins and other ECM proteins are initially organized in the ILM and
52 how the ILM directs the organization of the retina remains unclear.

53 In addition to β1-Integrin, the transmembrane glycoprotein dystroglycan functions as
54 a receptor for laminins and other ECM proteins through its extracellular α-subunit.
55 Dystroglycan connects to the actin cytoskeleton through the intracellular domain of its
56 transmembrane β-subunit, which is part of the dystrophin glycoprotein complex (Moore
57 and Winder, 2010). Mutations disrupting the glycosylation of dystroglycan affect its
58 binding to Laminin G (LG)-domain containing ECM proteins and lead to a form of
59 congenital muscular dystrophy termed dystroglycanopathy (Taniguchi-Ikeda et al.,
60 2016). The most severe forms, Muscle-Eye-Brain disease (MEB) and Walker Warburg
61 Syndrome (WWS), are accompanied by cortical malformation (type II lissencephaly),
62 cerebellar abnormalities, and retinal dysplasias (Dobyns et al., 1989).

63 Brain malformations in dystroglycanopathies reflect the critical role that dystroglycan
64 plays in maintaining the architecture of the neuroepithelial scaffold (Moore et al., 2002;
65 Myshrall et al., 2012). Focal regions of retinal dysplasia have also been observed In
66 mouse models of dystroglycanopathy, with ectopic cells protruding through the ILM
67 (Takeda et al., 2003; Lee et al., 2005; Satz et al., 2008; Chan et al., 2010; Takahashi et
68 al., 2011). In *Xenopus*, morpholino depletion of *dystroglycan* results in micropthalmia,
69 degeneration of the ILM, and abnormal positioning of photoreceptors, bipolar cells, and

retinal ganglion cells (Lunardi et al., 2006). However, several important questions regarding the role of dystroglycan in mammalian retinal development remain unaddressed. First, what is the underlying cause of retinal dysplasia in dystroglycanopathy? Second, is dystroglycan required for the proper migration and lamination of specific subtypes of retinal neurons? Third, how does the loss of dystroglycan affect axon guidance, dendritic stratification and mosaic spacing in the retina? Finally, how do retinal dysplasias in models of dystroglycanopathy affect the function of the retina?

Here, using multiple genetic models, we identify a critical role for dystroglycan in multiple aspects of retinal development. We show that dystroglycan within the neuroepithelium is critical for maintaining the structural integrity of the ILM. We provide *in vivo* evidence that dystroglycan's maintenance of the ILM is required for proper neuronal migration, axon guidance, formation of synaptic lamina, and the survival of multiple retinal neuron subtypes. Surprisingly, spontaneous retinal activity appears unperturbed, despite the dramatic disruption in inner retinal development. Together, these results provide critical insight into how dystroglycan directs the proper functional assembly of retinal circuits.

Material and Methods

Experimental Design and Statistical Analysis

Mice were maintained on mixed genetic backgrounds and were used irrespective of sex. All phenotypic analysis was conducted with n≥3 animals obtained from at least two different litters of mice. Statistical analysis was performed using JMP Pro 13.0 software

93 (SAS Institute). Comparison between two groups was analyzed using a Student's t-test.
94 Comparison between two or more groups was analyzed using a Two-Way ANOVA and
95 Tukey post-hoc test. Comparison of retinal wave parameters was analyzed using a
96 Wilcoxon Rank Sums test. The significance threshold was set at 0.05 for all statistical
97 tests. * indicates $p<0.05$; ** indicates $p<0.01$; *** indicates $p<0.001$.

98 **Animals**

99 Animal procedures were approved by OHSU Institutional Animal Care and Use
100 Committee and conformed to the National Institutes of Health *Guide for the care and*
101 *use of laboratory animals*. Animals were euthanized by administration of CO_2. The day
102 of vaginal plug observation was designated as embryonic day 0 (e0) and the day of birth
103 in this study was designated as postnatal day 0 (P0). The generation and genotyping
104 protocols for $ISPD^{L79*/L79*}$ (Wright et al., 2012), $DG^{F/F}$ (Moore et al., 2002) and $DG^{\beta cyt}$
105 (Satz et al., 2009) mice have been described previously. The presence of the cre allele
106 in $Sox2^{Cre}$ (Hayashi et al., 2002), $Six3^{Cre}$ (Furuta et al., 2000), $Isl1^{Cre}$ (Yang et al., 2006)
107 and $Nestin^{Cre}$ mice (Tronche et al., 1999) was detected by generic cre primers.
108 $ISPD^{+/L79*}$, $DG^{\beta cyt/+}$, and $DG^{F/+}$; $Six3^{Cre}$ or $DG^{F/+}$ age matched littermates were used as
109 controls.

110 **Tissue Preparation and Immunohistochemistry**

111 Embryonic retinas were left in the head and fixed overnight at 4°C in 4% PFA and
112 washed in PBS for 30 minutes. Heads were equilibrated in 15% sucrose overnight and
113 flash frozen in OCT medium. Postnatal retinas were dissected out of the animal and the
114 lens was removed from the eyecup. Intact retinas were fixed at room temperature for 30
115 minutes in 4% PFA. Retinas were washed in PBS for 30 minutes and equilibrated in a

116 sequential gradient of 10%, sucrose, 20% sucrose and 30% sucrose overnight. Tissue
117 was sectioned on a cryostat at 16-25um. Tissue sections were blocked in a PBS
118 solution containing 2% Normal Donkey Serum and 0.2% Triton for 30 minutes, and
119 incubated in primary antibody overnight at 4°C. Sections were washed for 30 minutes
120 and incubated in secondary antibody in a PBS solution containing 2% Normal Donkey
121 Serum for 2-4 hours. Sections were incubated in DAPI to stain nuclei for 10 minutes,
122 washed for 30 minutes, and mounted using Fluoromount medium. The source and
123 concentration of all antibodies utilized in this study are listed in Table 1.

124 **Wholemount retinal staining**

125 Postnatal retinas were dissected out of the animal and the lens was removed from
126 the eyecup. Intact retinas were fixed at room temperature for 30 minutes in 4% PFA.
127 Retinas were incubated in primary antibody diluted in PBS solution containing 2%
128 Normal Donkey Serum and 0.2% Triton for two days at 4°C. Retinas were washed in
129 PBS for one day and incubated in secondary antibody diluted in PBS solution containing
130 2% Normal Donkey Serum for two days at 4°C, washed for one day in PBS and
131 mounted using Fluoromount medium.

132 **Microscopy**

133 Imaging was performed on a Zeiss Axio Imager M2 upright microscope equipped
134 with an ApoTome.2. Imaging of synapses was performed on a Zeiss Elyra PS.1 with
135 LSM 710 laser-scanning confocal Super-Resolution Microscope with AiryScan. Imaging
136 of retinal waves was performed on a Nikon TiE inverted microscope with full
137 environmental chamber equipped with a Yokogawa CSU-W1 spinning disk confocal
138 unit.

139 **Quantification of cell number and mosaic spacing**

140 For each experiment, 3-4 locations per retina at the midpoint of each lobe were
141 sampled. Cell counts of horizontal cells (Calbindin), apoptotic cells (Cleaved Caspase-3,
142 P0), and starburst amacrine cells (ChAT) were obtained from 500 x 500 μm images and
143 quantified in FIJI. Cell counts of apoptotic cells (Cleaved Caspase-3, e16) and ganglion
144 cells (RPBMS) were obtained from 250 x 250 μm images and quantified in FIJI.
145 Analysis of retinal mosaics (Calbindin, ChAT) were conducted on 500 x 500 μm images
146 by measuring the X-Y coordinates for each cell and Voronoi domains were calculated in
147 FIJI and nearest neighbor measurements calculated with WinDRP. Cell counts of
148 proliferating cells (PH3 positive, e13, e16) were done by counting the number of positive
149 cells in mid-retinal 20μm sections.

150

151 **Live cell imaging and analysis**

152 Retinas from P1 *DG$^{F/+}$; Six3^{cre}; R26-LSL-GCaMP6f* and *DG$^{F/-}$; Six3^{cre}; R26-LSL-*
153 *GCaMP6f* were dissected into chilled Ames' Medium (Sigma) buffered with sodium
154 bicarbonate and bubbled with carbogen gas (95% O_2, 5% CO_2). The retinas were
155 dissected out of the eyecup, mounted RGC side up on cellulose membrane filters
156 (Millipore) and placed in a glass-bottom petri dish containing Ames' Medium. A platinum
157 harp was used to stabilize the filter paper during imaging. Imaging was performed at
158 30°C using a 10x0.45 Plan Apo Air objective with a field of 1664 by 1404 μm with a 3Hz
159 imaging timeframe. The field was illuminated with a 488 nm laser. 3-4 retinal fields were
160 imaged per retina, and each field of retina was imaged for a two-minute time series
161 using a 300ms exposure and each field was sampled 3-5 times per imaging session.

162 Thirty representative control and thirty representative mutant time series were
163 randomly selected for analysis. Only waves that initiated and terminated within the
164 imaging field were used for analysis. To measure wave area, movies were manually
165 viewed using FIJI frame by frame to determine the start and end frame of a wave. A Z-
166 Projection for maximum intensity was used to create an image with the entire wave, and
167 the boundary of the wave was manually traced to determine the area. Wave area per
168 time was calculated by dividing the area of the wave by the duration in seconds of the
169 wave. Any wave lasting less than 2 seconds was not used in analysis, consistent with
170 previous studies (Blankenship et al., 2009).
171

172 **Results**
173
174 **Dystroglycan is required for inner limiting membrane integrity**

175 Dystroglycan plays a critical role in the developing cortex, where it anchors radial
176 neuroepithelial endfeet to the basement membrane along the pial surface. In the
177 absence of functional dystroglycan, disruptions in the cortical basement membrane and
178 detachment of neuroepithelial endfeet lead to profound neuronal migration phenotypes
179 (Moore et al., 2002; Myshrall et al., 2012). In the adult retina, dystroglycan is present in
180 blood vessels, in RGCs, at ribbon synapses in the OPL, and at the ILM, which serves as
181 a basement membrane that separates the neural retina from the vitreous space
182 (Montanaro et al., 1995; Omori et al., 2012). However, the role of dystroglycan in
183 regulating neuronal migration, axon guidance or dendritic stratification of specific cell
184 types during retinal development has not been examined in a comprehensive manner.
185 To address this open question, we first examined the expression pattern of dystroglycan

186 in the developing retina. Using immunohistochemistry, we observed dystroglycan
187 expression along radial processes that span the width of the retina, and its selective
188 enrichment at the ILM from embryonic ages (e13) through birth (P0) (Figure 1A). These
189 processes are likely a combination of neuroepithelial cells and the basal process of
190 migrating RGCs. Loss of staining in retinas from an epiblast-specific *dystroglycan*
191 conditional knockout (*DG*$^{F/-}$*; Sox2*^{cre}) confirmed the specificity of this expression pattern
192 (Figure 1B).

193 The first step in the assembly of basement membranes is the recruitment of laminin
194 polymers to the cell surface by sulfated glycolipids, followed by the stabilization of
195 laminin polymers by transmembrane receptors (Yurchenco, 2011). To determine
196 whether dystroglycan is required for the initial formation of the ILM during retinal
197 development, we utilized two complementary genetic models. *ISPD*$^{L79*/L79*}$ mutants,
198 previously identified in a forward genetic screen, lack the mature glycan chains required
199 for dystroglycan to bind ligands such as laminin and are a model for severe
200 dystroglycanopathy (Wright et al., 2012). *DG*$^{F/-}$*; Sox2*^{cre} conditional mutants lack
201 dystroglycan in epiblast-derived tissues, including all retinal tissue, and were utilized to
202 confirm that phenotypes observed in *ISPD*$^{L79*/L79*}$ mice are dystroglycan dependent. The
203 enrichment of laminin at the ILM appeared normal in early retinal development at e13 in
204 both *ISPD*$^{L79*/L79*}$ and *DG*$^{F/-}$*; Sox2*^{cre} mutants (Figure 1C-E), indicating that dystroglycan
205 is not required for the initial formation of the ILM. However, at e16, we observed a loss
206 of laminin staining and degeneration of the ILM across the entire surface of the retina in
207 *ISPD*$^{L79*/L79*}$ and *DG*$^{F/-}$*; Sox2*^{cre} mutants (Figure 1D-F). The loss of ILM integrity in
208 *ISPD*$^{L79*/L79*}$ and *DG*$^{F/-}$*; Sox2*^{cre} mutants was accompanied by the inappropriate

209 migration of retinal neurons, resulting in the formation of an ectopic layer of neurons
210 protruding into the vitreous space.

211 Following the initial polymerization of laminin on cell surfaces, additional ECM
212 proteins bind and crosslink the nascent basement membrane to increase its stability
213 and complexity. Examination of *ISPD*$^{L79*/L79*}$ and *DG*$^{F/-}$*; Sox2*^{cre} mutant retinas at P0
214 revealed a loss of the ECM proteins Collagen IV (red), and Perlecan (green), coinciding
215 with the disruptions in Laminin (purple) (Figure 2A, B**,** C). These data suggest that while
216 dystroglycan is not required for the initial formation of the ILM, it is essential for its
217 maturation and maintenance. Furthermore, dystroglycan is critical for the ILM to
218 function as a structural barrier to prevent the ectopic migration of neurons into the
219 vitreous space.

220

221 **Dystroglycan is required for vascular and optic fiber layer development**

222 The hyaloid vasculature in the embryonic retina normally regresses as astrocytes
223 and the retinal vascular plexus emerge through the optic nerve head beginning around
224 birth (Fruttiger, 2007). Previous studies have found that defects in ILM integrity disrupt
225 the emergence and migration of astrocytes and the retinal vasculature (Lee et al., 2005;
226 Edwards et al., 2010; Takahashi et al., 2011; Tao and Zhang, 2016). In agreement with
227 these findings, we observe that at embryonic ages in *ISPD*$^{L79*/L79*}$ mutant retinas, the
228 hyaloid vasculature becomes embedded within the ectopic retinal neuron layer at e16
229 (Figure 3A), and fails to regress at P0 (Figure 3B). In addition, the emergence of the
230 retinal vasculature and astrocytes is stunted in *ISPD*$^{L79*/L79*}$ mutants (Figure 3B).

231 We have shown previously that the organization of the basement membrane by
232 dystroglycan provides a permissive growth substrate for axons in the developing spinal
233 cord (Wright et al., 2012). In addition, contact with laminin in the ILM stabilizes the
234 leading process of newly generated RGCs to direct the formation of the nascent axon
235 (Randlett et al., 2011). These axons remain in close proximity to the ILM as they extend
236 centrally towards the optic nerve head, forming the optic fiber layer (OFL). Therefore,
237 we examined whether the disruptions in the ILM affected the guidance of RGC axons in
238 *ISPD*$^{L79*/L79*}$ and *DG*$^{F/-}$*; Sox2*^{cre} mutants. At e13, axons in both control and mutant
239 retinas formed a dense and continuous network in the basal retina, directly abutting the
240 ILM (Figure 4A). In contrast, at e16 (Figure 4B) and P0 (Figure 4C), RGC axons in
241 *ISPD*$^{L79*/L79*}$ and *DG*$^{F/-}$*; Sox2*^{cre} mutants were disorganized, exhibiting both
242 defasciculation (asterisks) and hyperfasciculation (arrowheads).
243 To gain further insight into the specific defects that occur in RGC axons, we used a
244 flat mount retina preparation. Regardless of their location in the retina, all RGCs orient
245 and extend their axons towards the center of the retina, where they exit the retina
246 through the optic nerve head (Bao, 2008). In control retinas at e16 (Figure 4D, left
247 panel) and P0 (Figure 4E, left panel) axons traveled towards the optic nerve head in
248 fasciculated, non-overlapping bundles. In contrast, we frequently observed
249 defasciculated RGC axons that grew in random directions without respect to their
250 orientation to the optic nerve head in both *ISPD*$^{L79*/L79*}$ and *DG*$^{F/-}$*; Sox2*^{cre} mutants.
251 Together, these data show that proper growth and guidance of RGC axons to the optic
252 nerve head requires dystroglycan to maintain an intact ILM as a growth substrate.
253

254 **Dystroglycan is required for axonal targeting, dendritic lamination, and cell**
255 **spacing in the postnatal retina**

256 Our results in *ISPD*$^{L79*/L79*}$ and *DG*$^{F/-}$*; Sox2*^{cre} mutants demonstrate that
257 dystroglycan is required for ILM integrity and to prevent the ectopic migration of neurons
258 into the vitreous (Figure 1). However, the specific neuronal subtypes affected in models
259 of dystroglycanopathy are unknown, and the role of dystroglycan in regulating postnatal
260 aspects of retinal development has not been examined. The synaptic layers of the retina
261 develop postnatally, with tripartite synapses between the photoreceptors, bipolar cells
262 and horizontal cells forming in the OPL, and synapses between bipolar cells, amacrine
263 cells and retinal ganglion cells forming in the IPL. The development of these synaptic
264 layers requires the precise stratification of both axons and dendrites that occurs
265 between P0 and P14. Since *ISPD*$^{L79*/L79*}$ and *DG*$^{F/-}$*; Sox2*^{cre} mutant mice exhibit
266 perinatal lethality, we deleted *dystroglycan* selectively from the early neural retina using
267 a *Six3*^{Cre} driver (Furuta et al., 2000) (Figure 5A).

268 Analysis of *DG*$^{F/-}$*; Six3*^{cre} retinas confirmed that dystroglycan protein was lost along
269 the neuroepithelial processes and at the ILM (Figure 5B). We next confirmed that *DG*$^{F/-}$*;*
270 *Six3*^{cre} mice recapitulated the retinal phenotypes identified in *ISPD*$^{L79*/L79*}$ and *DG*$^{F/-}$*;*
271 *Sox2*^{cre} mice. We observed a degeneration of the ILM (laminin, purple) accompanied by
272 ectopic migration of neurons into the vitreous (Figure 5C), abnormal fasciculation and
273 guidance of RGC axons (Figure 5D), and defective emergence and migration of
274 astrocytes and the vascular plexus (Figure 5E). While fully penetrant, the ILM
275 degeneration and neuronal migration defects in *DG*$^{F/-}$*; Six3*^{cre} mice were milder than in
276 *DG*$^{F/-}$*; Sox2*^{cre} mice, exhibiting a patchiness that was distributed across the retina

277 (Figure 5F). The defects in *DG*$^{F/-}$*; Six3*^{cre} mice contrast the finding that conditional
278 deletion of *dystroglycan* with *Nestin*^{cre} does not affect the overall structure of the retina
279 (Satz et al., 2009). We find that this difference is likely due to the onset and pattern of
280 *Cre* expression, as recombination of a *Cre*-dependent reporter (*Rosa26-lox-stop-lox-*
281 *TdTomato; Ai9*) occurred earlier and more broadly in *Six3*^{Cre} mice than in *Nestin*^{cre} mice
282 (Figure 5A, data not shown).

283 *DG*$^{F/-}$*; Six3*^{cre} mice are healthy and survive into adulthood, allowing us to examine
284 the role of dystroglycan in postnatal retinal development. We analyzed *DG; Six3*^{cre}
285 retinas at P14 when migration is complete and the laminar specificity of axons and
286 dendrites has been established (Morgan and Wong, 1995). The overall architecture of
287 the ONL appeared unaffected by the loss of dystroglycan in *DG*$^{F/-}$*; Six3*^{cre} mice, and cell
288 body positioning of photoreceptors appeared similar to controls (Figure 6A). Within the
289 INL, the laminar positioning of rod bipolar cell bodies (PKC, Figure 6B), cone bipolar cell
290 bodies (SCGN, Figure 6C), horizontal cells (arrows, Calbindin, Figure 6E), and Müller
291 glia cell bodies (Figure 6H) and the targeting of their processes to the OPL appeared
292 normal in *DG*$^{F/-}$*; Six3*^{cre} mutants. However, bipolar cell axons that are normally confined
293 to the synaptic layers in the IPL, and Müller glia processes that are normally
294 concentrated at the ILM both extended aberrant projections into the ectopic clusters
295 (Figure 6B-C, H).

296 In contrast to the normal laminar architecture of the outer retina, the inner retina
297 was disorganized in *DG*$^{F/-}$*; Six3*^{cre} mutants. Subsets of amacrine and ganglion cells
298 labeled by ChAT (starburst amacrine cells, Figure 6D), calbindin (Figure 6E), and
299 calretinin (Figure 6F) that are normally confined to the INL and GCL were present in the

300 ectopic clusters that protrude into the vitreous space. Glycinergic amacrine cells (GlyT1,
301 Figure 6G), whose cell bodies are normally found in a single layer within the INL, were
302 also present within ectopic clusters. Compared to the OPL, which appeared grossly
303 normal, dendritic stratification within the IPL in *DG*$^{F/-}$; *Six3*^{cre} mutant retinas was
304 disrupted. The laminated dendritic strata appeared expanded (Figure 6D), fragmented
305 (Figure 6D-F) and occasionally lacked an entire lamina (Figure 6E). These defects were
306 restricted to regions of the retina where ectopic neuronal clusters were present,
307 whereas regions of the *DG*$^{F/-}$; *Six3*^{cre} mutant retina with normal cellular migration and
308 lamination also had normal dendritic stratification (Figure 5F). These results
309 demonstrate that the ectopic clusters consisted of multiple subtypes of amacrine cells
310 and ganglion cells that normally reside in the INL and GCL, and that the disorganization
311 of the dendritic strata are likely secondary to the cell migration defects.

312 Over the course of retinal development, multiple cell types, including horizontal
313 cells and amacrine cells, develop mosaic spacing patterns that ensure cells maintain
314 complete and non-random coverage over the surface of the retina (Wassle and
315 Riemann, 1978). This final mosaic pattern is established by both the removal of excess
316 cells through apoptosis and the lateral dispersion of “like-subtype” cells via homotypic
317 avoidance mechanisms (Kay et al., 2012; Li et al., 2015). To determine whether the
318 defects in establishing proper laminar positioning of retinal subtypes in *DG*$^{F/-}$; *Six3*^{cre}
319 mutants extends to mosaic spacing, we performed nearest neighbor analysis. For
320 horizontal cells, which exhibit normal lamination in *DG*$^{F/-}$; *Six3*^{cre} mutant retinas, we
321 observed a small, but significant reduction in the number of cells (Figure 7A-B, Two-
322 Way ANOVA, $p<0.0001$, Tukey HSD post-hoc test ***$p<0.0001$). Despite the reduction

323 in horizontal cell number, nearest neighbor curves between controls and mutants are
324 the same shape, indicating that horizontal cell mosaics are maintained in dystroglycan
325 mutants (Figure 7A-B).

326 ChAT positive starburst amacrine cells are present in two distinct lamina that form
327 mosaic spacing patterns independent from one another. Consistent with this, ChAT
328 labeled cells in the INL showed normal mosaic cell spacing (Figure 7C, top, Figure 7D,
329 top, Two-Way ANOVA, Tukey HSD post-hoc test *p=0.0494). In contrast, the GCL
330 contained prominent ChAT positive clusters that corresponded to the ectopic
331 protrusions that extend into the vitreous, resulting in a decrease in cell spacing as
332 determined by nearest neighbor analysis (Figure 7C, bottom, Figure 7D, bottom, Two-
333 Way ANOVA, p<0.0001, Tukey HSD post-hoc test ***p<0.0001). These results
334 demonstrate that laminar migration defects in $DG^{F/-}$; $Six3^{cre}$ mutants degrade the mosaic
335 spacing of cells in the GCL, and that contact with an intact ILM is likely required for the
336 proper lateral dispersion of these cells.

337

338 **Deletion of dystroglycan leads to a loss of photoreceptors, horizontal cells and**
339 **ganglion cells**

340 During development, normal physiological apoptotic cell death during the first two
341 postnatal weeks plays an important role in retinal maturation (Young, 1984). This
342 process is critical for establishing the proper numbers and spacing of some subtypes of
343 cells across the mature retina, as well as removing cells that fail to connect to
344 appropriate synaptic targets (Braunger et al., 2014). Degeneration of the ILM during
345 development can lead to a reduction in the number of ganglion cells, and previous

346 analysis of dystroglycanopathy mutants has noted thinning of the retina (Halfter et al.,
347 2005; Lee et al., 2005; Satz et al., 2008; Chan et al., 2010; Takahashi et al., 2011). In
348 agreement with these results, we observed that the retinas of *DG*$^{F/-}$*; Six3*^{cre} mutants are
349 thinner (Figure 6, 8). However, the specific cell types affected by the loss of
350 dystroglycan in the retina are unknown.

351 To investigate the mechanism by which loss of dystroglycan contributes to retinal
352 thinning, we began by measuring the distance between the edges of the inner and outer
353 retina in control and *DG*$^{F/-}$*; Six3*^{cre} mutants by DAPI staining and found that there was a
354 significant reduction in overall retinal thickness by approximately 20% in mutants
355 (Figure 8A, blue, Figure 8B, t test, p=0.0039). We next investigated which specific cell
356 types contribute to retinal thinning. In the outer retina, the thickness of the photoreceptor
357 layer (recoverin, Figure 8A, green, Figure 8C, t-test, p=0.0163) was reduced by
358 approximately 20% and the density of horizontal cells had a small, yet significant
359 reduction in *DG*$^{F/-}$*; Six3*^{cre} mutants (calbindin, Figure 8G, t-test, p=0.0112). In contrast,
360 the thickness of the bipolar cell layer (Chx10, Figure 8A, purple, Figure 8D, t-test,
361 p>0.05) was normal. In the inner retina, there was a 50% reduction in the density of
362 ganglion cells (Figure 8H, I, t-test, p<0.0001), while the density of ChAT+ starburst
363 amacrine cells in both the INL and GCL was normal in *DG*$^{F/-}$*; Six3*^{cre} mutants (Figure 8E,
364 F, t-test, p>0.05). Thus, a reduction in the number of photoreceptors, horizontal cells
365 and RGCs contribute to the overall thinning of *DG*$^{F/-}$*; Six3*^{cre} retinas.

366 To determine whether the reduction in photoreceptors, horizontal cells and RGCs in
367 the absence of dystroglycan was due to defects in proliferation of retinal progenitors, we
368 examined phospho-Histone H3 (PH3) staining at embryonic ages. PH3 positive mitotic

369 progenitors were localized along the apical surface of the retina, and were present at
370 the normal number in *ISPD*$^{L79*/L79*}$ mutants at e13 and e16 and (Figure 9 A, B, t-test,
371 p>0.05). To determine whether the reduced number of neurons in mutant retinas was
372 due to increased apoptosis, we quantified the number of caspase-3 positive cells. At
373 e13, we observed no difference between in the number of caspase-3 positive cells in
374 *ISPD*$^{L79*/L79*}$ mutants and controls (data not shown). In contrast, there was a significant
375 increase in caspase-3 positive cells in *ISPD*$^{L79*/L79*}$ mutants at e16 (Figure 9D, t-test,
376 p<0.0001) and P0 (Figure 9C, D, t-test, p<0.0001) that was restricted to the ganglion
377 cell layer. Similarly, we observed an increased number of cleaved caspase-3 positive
378 cells in the ganglion cell layer in *DG*$^{F/-}$*; Six3*^{cre} mutants at P0 (Figure 9C, D, t-test,
379 p=0.0279). These results led us to conclude that the loss of RGCs in *DG*$^{F/-}$*; Six3*^{cre}
380 mutants is due to increased apoptotic cell death.
381
382 **Dystroglycan functions non-cell autonomously as an extracellular scaffold in the**
383 **developing retina**
384 We next sought to provide mechanistic insight into how dystroglycan regulates
385 retinal development *in vivo*. In the cerebral cortex, the loss of dystroglycan results in
386 breaches of the pial basement membrane and detachment of neuroepithelial endfeet
387 from the pial surface, depriving neurons of a migratory scaffold. In addition, the cortical
388 basement membrane defects cause the mis-positioning of Cajal-Retzius cells, which are
389 the source of Reelin that regulates somal translocation of neurons as they detach from
390 the neuroepithelial scaffold (Nakagawa et al., 2015). Deletion of *dystroglycan*
391 specifically from postmitotic cortical neurons does not result in a migration phenotype

392 (Satz et al., 2010), supporting a model in which the cortical migration phenotypes arise
393 due to disrupted interactions between the basement membrane and neuroepithelial
394 scaffold. In contrast to the cerebral cortex, the basal migration of RGCs does not involve
395 contact with the neuroepithelial scaffold. Instead, newly born RGCs migrate via somal
396 translocation using an ILM-attached basal process that eventually becomes the nascent
397 axon (Randlett et al., 2011; Icha et al., 2016). Dystroglycan's expression in ILM-
398 attached basal processes (Figure 1A) and RGCs (Montanaro et al., 1995) and the
399 restriction of neuronal migration and axon guidance defects to the GCL raise the
400 possibility that dystroglycan could be functioning cell-autonomously in the basal
401 processes of newly born RGCs. To test this possibility, we generated *DG*$^{F/-}$*; Isl1*^{cre}
402 conditional knockouts. *Islet1* is expressed in the majority of ganglion cells as they
403 differentiate from the retinal progenitor pool (Pan et al., 2008b). Analysis of *Isl1*^{cre} mice
404 at e13 confirmed recombination occurs in the majority of newly born ganglion cells, but
405 not in neuroepithelial progenitors (Figure 10A). Interestingly, dystroglycan protein
406 expression in *DG*$^{F/-}$*; Isl1*^{cre} mutants was not altered compared to controls, suggesting
407 that RGCs do not provide a significant source of dystroglycan at the ILM (Figure 10B).
408 Examination of *DG*$^{F/-}$*; Isl1*^{cre} mutants indicated that deletion of *dystroglycan* selectively
409 from RGCs did not affect ILM integrity (Figure 10C). Neuronal migration (Figure 10C, E
410 and F), axon guidance (Figure 10C and D) and the stratification of dendrites in the IPL
411 (Figures 10 E and F) all appeared normal in *DG*$^{F/-}$*; Isl1*^{cre} mutants. These results
412 demonstrate that dystroglycan is not required within RGCs themselves during retinal
413 development.

414 Dystroglycan consists of two subunits that can play distinct roles in the overall
415 function of the protein. The extracellular α-subunit is heavily glycosylated and functions
416 as an extracellular scaffold by binding to extracellular matrix components such as
417 laminin. The β-subunit contains a transmembrane and intracellular domain, and can
418 bind directly to the intracellular scaffolding protein dystrophin and other modifiers of the
419 actin cytoskeleton, as well as initiate intracellular signaling cascades (Moore and
420 Winder, 2010). The intracellular domain of dystroglycan is required for the localization of
421 dystrophin to the ILM, and mice lacking the intracellular domain of dystroglycan ($DG^{-/\beta cyt}$)
422 (Satz et al., 2009) or the predominant retinal isoform of dystrophin (Mdx^{3Cv}) (Blank et al.,
423 1999) have abnormal scotopic electroretinograms, suggesting a defect in retinal
424 function. While these mice do not have any disruptions in the ILM or gross
425 malformations in the retina, whether dystroglycan signaling through dystrophin is
426 required for neuronal migration, axon guidance or dendritic stratification has not been
427 examined. Consistent with the original report, examination of the ILM and overall
428 architecture of the retina is normal in $DG^{-/\beta cyt}$ mice (Figure 11A). In addition, we find that
429 neuronal migration, axon guidance and stratification of dendritic lamina are unaffected
430 in $DG^{-/\beta cyt}$ mice (Figure 11A-D). Therefore, intracellular signaling, including through
431 dystrophin, is not required for these aspects of retinal development. Taken together with
432 our results in $DG^{F/-}$; $Isl1^{cre}$ mutants, these findings indicate that dystroglycan primarily
433 functions within neuroepithelial cells as an extracellular scaffold to regulate the
434 structural integrity of the ILM. The progressive degeneration of the ILM then leads to
435 secondary defects including aberrant migration, axon guidance and dendritic
436 stratification that primarily affect the inner retina.

437

438 **Dystroglycan is dispensable for the generation of spontaneous retinal waves**

439 One of the critical functions for laminar targeting in neural circuit development is to
440 ensure that the axons and dendrites of appropriate cell types are in physical proximity to
441 one another during synaptogenesis. In addition to regulating the laminar positioning of
442 neurons in the cortex and retina, dystroglycan is required for the development of a
443 subset of inhibitory synapses in the brain (Fruh et al., 2016). Therefore, we investigated
444 the possibility that the loss of dystroglycan disrupts synapse formation in the retina.
445 Previous studies have shown that ribbon synapses in the OPL are dysfunctional in the
446 absence of dystroglycan or its ligand pikachurin (Sato et al., 2008). These synapses are
447 normal at the resolution of light microscopy, but electron microscopy reveals that
448 dystroglycan and pikachurin are required for the insertion of bipolar cell dendrite tips
449 into ribbon synapse invaginations (Omori et al., 2012). Consistent with these results, we
450 found that pre- and post-synaptic markers for ribbon synapses are present in $DG^{F/-}$;
451 $Six3^{cre}$ mutants (Figure 12A). In the inner retina, markers for excitatory synapses
452 (VGLUT1, Figure 12B) and inhibitory synapses (VGAT, Figure 12C) were present in the
453 IPL, and were also present in the mis-localized ectopic cell clusters that protrude into
454 the vitreous (asterisks). This finding is similar to a recent study in which mice lacking the
455 Cas family of intracellular adaptor proteins express synaptic markers localized to
456 aberrant neuronal ectopia that protrude into the vitreous (Riccomagno et al., 2014).
457 These results suggest that mis-laminated neurons in the retina are still able to recruit
458 synaptic partners, despite their abnormal location.

459 The presence of synaptic markers in ectopic neuronal clusters in the inner retina
460 does not guarantee normal function of these neurons. Recording synaptic activity in
461 RGCs in response to light stimuli in *DG*$^{F/-}$*; Six3*^{cre} mutants is not feasible due to the
462 requirement for dystroglycan at photoreceptor ribbon synapses. We instead analyzed
463 retinal waves, which are spontaneous bursts of activity that propagate across the retina
464 prior to eye opening and are independent of light stimulation. During early postnatal
465 development, these waves are initiated by acetylcholine (ACh) release from starburst
466 amacrine cells and propagate along the starburst amacrine cell network prior to
467 transmission to RGCs (Xu et al., 2016). In *DG*$^{F/-}$*; Six3*^{cre} mutants, ChAT positive
468 starburst amacrine cells are present in normal numbers, and while they are normally
469 localized and mosaically spaced in the INL, they are disorganized in the GCL.
470 Therefore, we expected that these defects might affect the propagation of retinal waves
471 through the starburst amacrine cell and RGC network. As disruptions in the ILM in *DG*$^{F/-}$
472 *; Six3*^{cre} mutants would lead to unequal bulk loading of cell permeable calcium
473 indicators, we utilized the genetically-encoded calcium indicator GCaMP6f crossed onto
474 the *DG; Six3*^{cre} line to visualize retinal waves.

475 Retinal waves in control *DG*$^{F/+}$*; Six3*^{cre}*; R26-LSL-GCaMP6f* retinas at P1-P2 were
476 robust and had similar spatiotemporal features (area, rate of propagation, refractory
477 period) to waves measured using cell-permeable calcium indicators (Arroyo and Feller,
478 2016). Consistent with previous reports, there is a broad distribution of wave area in
479 control retinas (Figures 13A, C, Movie 1). Neighboring waves do not overlap with one
480 another, but rather tile the retinal surface during the two-minute imaging period. To our
481 surprise, retinal waves were present and appeared grossly normal in *DG*$^{F/-}$*; Six3*^{cre}*;*

482 *R26-LSL-GCaMP6f* mutants (Figure 13B, Movie 2). Waves in control and mutant retinas
483 exhibited a similar distribution in wave area (Figure 13C), and the average wave area
484 showed no statistical difference. The rate of wave propagation showed a similar
485 distribution between controls and mutants (Figure 13D). The average rate of wave
486 propagation showed a small, but statistically significant, decrease (Wilcoxon Rank Sum
487 test, p=0.0493). Thus, despite the dramatic disorganization of ChAT positive starburst
488 amacrine cells in the GCL of $DG^{F/-}$; $Six3^{cre}$ mutants, the generation and propagation of
489 retinal waves persisted.
490

491 **Discussion**
492
493 While defects in retinal structure and function are observed in both human patients
494 and mouse models of dystroglycanopathy, the mechanism of dystroglycan function in
495 the mammalian retina and the consequence of its loss on specific cell types are poorly
496 understood (Takeda et al., 2003; Lee et al., 2005; Satz et al., 2008; Satz et al., 2009;
497 Chan et al., 2010; Takahashi et al., 2011). Our study establishes a critical role for
498 dystroglycan in maintaining the integrity of the ILM, which is required for intra-retinal
499 axon guidance and establishing laminar architecture and mosaic spacing in the inner
500 retina. Mechanistically, we show that dystroglycan functions non-cell autonomously as
501 an extracellular scaffold, as mice with selective deletion of *dystroglycan* from postmitotic
502 RGCs (*DG;* $Isl1^{cre}$) and mice lacking the intracellular domain of dystroglycan ($DG^{-/\beta cyt}$)
503 appear phenotypically normal. Despite the dramatic disruptions in cellular lamination in
504 the GCL and dendritic stratification in the IPL in *DG;* $Six3^{cre}$ mutants, dystroglycan

505 appears dispensable for the formation of synapses and the generation of spontaneous,
506 light-independent activity in the retina.
507
508 **Requirement for dystroglycan at the ILM during retinal development.**
509 Using two genetic models for the complete loss of functional dystroglycan (*ISPD*^{L79*}
510 and *DG; Sox2*^{Cre}), we demonstrated that after the ILM forms, it rapidly degenerates in
511 the absence of dystroglycan. These results suggest that dystroglycan is not required for
512 the formation of the nascent ILM, but rather plays a critical role in maintaining ILM
513 structure as it expands to accommodate the growing retina. Recruitment of laminin is a
514 critical early step in the assembly of the ILM, and several laminin mutants have similar
515 disruptions in ILM integrity (Edwards et al., 2010; Pinzon-Duarte et al., 2010;
516 Gnanaguru et al., 2013). In contrast to *Xenopus*, where depletion of *dystroglycan* results
517 in degeneration of both the ILM in the inner retina and Bruch's membrane in the outer
518 retina, Bruch's membrane is unaffected by the loss of *dystroglycan* or isoforms of
519 *Laminin* (Lunardi et al., 2006; Pinzon-Duarte et al., 2010). Mice lacking *β-1 Integrin* in
520 the retina exhibit a similar defect to *dystroglycan* mutants, raising the possibility that
521 these laminin receptors may be functionally redundant (Riccomagno et al., 2014).
522 Surprisingly however, mice in which both *dystroglycan* and *β-1 Integrin* are deleted from
523 the retina (*DG*; *ItgB1*; *Six3*^{Cre}) still formed an ILM at e13, and the subsequent
524 degeneration of the ILM was indistinguishable from *DG*; *Six3*^{Cre} mutants (unpublished
525 observations). Therefore, sulfated glycolipids alone are likely sufficient for the
526 recruitment of laminin during the initial formation of the ILM.
527

528 **The ILM is required for neuronal migration and axon outgrowth in the retina**

529 In the developing cortex, the loss of functional dystroglycan leads to degeneration
530 of the radial glia processes and ectopic clustering of reelin-secreting Cajal-Retzius
531 neurons, which are thought to be the principal drivers of structural brain defects in
532 dystroglycanopathies (Myshrall et al., 2012; Nakagawa et al., 2015; Booler et al., 2016).
533 Retinal neurons do not migrate along the neuroepithelial scaffold, and there is no cue
534 analogous to reelin to signal termination of migration, suggesting that while dystroglycan
535 functions primarily in neuroepithelial cells in the retina, the functional implications are
536 distinct from its role in cortical neuroepithelial cells. In the cortex of *dystroglycan*
537 deficient mice, the organization of neurons across all lamina is affected, whereas within
538 the retina, migration defects are restricted to amacrine cells and RGCs in the inner
539 retina. In contrast, migration defects in dystroglycan-deficient *Xenopus* retinas are more
540 widespread and also affect outer retinal neurons, likely reflecting the requirement for
541 dystroglycan at both the ILM and Bruch's membrane (Lunardi et al., 2006). What is the
542 driving force behind the selective localization of amacrine cells and RGCs to the ectopic
543 clusters that protrude into the vitreous in the mammalian retina? While the elimination of
544 RGCs does not affect the lamination of other neurons, other neurons will organize
545 themselves around mislocalized RGCs, resulting in an overall disorganization of retinal
546 lamination (Wang et al., 2001; Kay et al., 2004; Icha et al., 2016). In *dystroglycan*
547 mutants, RGCs that encounter the degenerating ILM and inappropriately migrate into
548 the vitreous may then actively recruit later born neurons such as amacrine cells to
549 inappropriate locations.

550 The establishment of retinal mosaics requires tangential migration that is regulated
551 by short range interactions between immature neurites of neighboring cells (Galli-Resta
552 et al., 1997; Reese et al., 1999; Galli-Resta et al., 2002; Huckfeldt et al., 2009). A key
553 feature of this process is that it requires homotypic cells to be localized within the same
554 lamina, and cells in which mosaic spacing is disrupted are no longer restricted to a two-
555 dimensional plane (Fuerst et al., 2008; Kay et al., 2012). In *dystroglycan* mutants, the
556 laminar organization and mosaic spacing is normal in horizontal cells and INL starburst
557 amacrine cells, but disrupted in starburst amacrine cells in the GCL. This defect is not
558 due to dystroglycan functioning within starburst amacrine cells, as mosaic spacing was
559 normal in *DG*; *Isl1*^{Cre} mutant retinas (data not shown). Rather, the selective defects in
560 mosaic spacing of GCL starburst amacrine cells suggests that this is likely a
561 consequence of disrupting the two-dimensional organization of the GCL. Alternatively,
562 mosaic spacing of cells within the GCL may require cues present in the ILM for their
563 tangential dispersion.

564 Basement membranes are highly dynamic structures that contain pro-axon growth
565 ECM molecules such as laminins and collagens, and also regulate the distribution of
566 secreted axon guidance cues (Halfter et al., 1987; Chai and Morris, 1999; Xiao et al.,
567 2011; Wright et al., 2012). A number of secreted cues direct intraretinal axon guidance
568 of RGCs. Deletion of Netrin (Deiner et al., 1997) specifically affects exit of RGC axons
569 through the optic nerve head, and deletion of Slits (Thompson et al., 2006) or Sfrps
570 (Marcos et al., 2015) leads to the invasion of RGC axons into the outer retina. In
571 contrast, the randomized growth and defasciculation of axons we observed in *ISPD*^{L79*}
572 and *DG*; *Six3*^{Cre} mutant retinas is more consistent with defects observed upon deletion

573 of adhesion receptors (Bastmeyer et al., 1995; Brittis et al., 1995; Ott et al., 1998).
574 These results suggest that dystroglycan primarily functions to organize the ILM as a
575 substrate for axonal adhesion.
576
577 **Loss of retinal neurons in the absence of dystroglycan**
578 While previous studies of mouse models of dystroglycanopathy have consistently
579 noted retinal thinning, it was unclear which retinal cell types were affected. Our
580 comprehensive analysis found that lack of dystroglycan led to reductions in
581 photoreceptor layer thickness, horizontal cell number, and RGC number (Figure 8).
582 Analysis of e13, e16 and P0 retinas from *ISPD*^{L79*} and *DG; Six3*^{cre} mutants indicated
583 that the loss of RGCs was not due to altered proliferation of retinal progenitors, but was
584 primarily due to increased apoptosis of cells in the GCL that preceded and extended
585 into the normal window of developmental apoptotic cell death. This increase in
586 apoptotic cell death did not persist in adult (P56) *DG; Six3*^{cre} mutants (data not shown),
587 suggesting it was likely restricted to the developing retina. Why are RGCs lost at such a
588 high rate in *DG; Six3*^{cre} mutants, while displaced amacrine cell number in the GCL
589 remains normal? One possibility is that RGCs are selectively affected since they are the
590 only cell type to project out of the retina. Indeed, we observed profound guidance
591 defects of RGCs at the optic chiasm in *ISPD*^{L79*} and *DG; Six3*^{cre} mutants (unpublished
592 observations). This result is similar to *Isl1* and *Brn3b* deficient mice, in which axon
593 growth defects at the optic chiasm precede an increase in RGC apoptosis (Gan et al.,
594 1999; Pan et al., 2008a). The death of RGCs whose axons fail to reach retinorecipient

595 regions of the brain is consistent with the need for target-derived factors to support their
596 survival, although the identity of these factors remains elusive.
597 While we did not observe increased caspase-3 reactivity in photoreceptors or
598 horizontal cells at P0, it is possible that the loss of cells occurred gradually during the
599 first two postnatal weeks. Dystroglycan is required for the proper formation of ribbon
600 synapses between photoreceptors, horizontal cells and bipolar cells in the OPL (Sato et
601 al., 2008; Omori et al., 2012). Therefore, the loss of appropriate synaptic contact in the
602 absence of dystroglycan may lead to the elimination of a proportion of photoreceptors
603 and horizontal cells.
604
605 **Persistence of retinal waves in the absence of dystroglycan**
606 The defects in lamination and dendritic stratification of starburst amacrine cells in
607 *DG; Six3^{cre}* mutants led us to hypothesize that this would affect their ability to generate
608 retinal waves. These waves are initiated by the spontaneous activity of starburst
609 amacrine cells, independent of light stimuli, allowing us to circumvent the requirement
610 for dystroglycan in proper transmission at ribbon synapses. Contrary to our
611 expectations, retinal waves were present and propagated normally in *DG; Six3^{cre}*
612 mutants (Figure 13). The persistence of retinal waves even in the context of disrupted
613 cellular organization supports the model that these waves are the product of volume
614 release of ACh from starburst amacrine cells that can trigger extra-synaptic responses
615 in cells that are not physically connected (Ford et al., 2012). Therefore, the relatively
616 normal organization of INL starburst amacrine cells may be sufficient to overcome the
617 disorganization of GCL starburst amacrine cells.

618

619 **Conclusion**

620 Retinal dysplasia and optic nerve hypoplasia are frequently observed in patients
621 with severe forms of dystroglycanopathy (Manzini et al., 2008). Using multiple mouse
622 models, we demonstrate that dystroglycan is required for multiple aspects of retinal
623 development. We show that dystroglycan functions within neuroepithelial cells in the
624 retina to regulate the structural integrity of a basement membrane (the ILM), which is
625 required for the coordination of neuronal migration, axon guidance and dendritic
626 stratification in the inner retina. In addition, we find that there is a significant loss of
627 photoreceptors, horizontal cells and almost 50% of RGCs due to increased apoptotic
628 cell death. Our data suggest that the disorganization of the inner retina resulting from
629 degeneration of the ILM is a key contributor to visual impairment in
630 dystroglycanopathies.

631

References

Arroyo DA, Feller MB (2016) Spatiotemporal Features of Retinal Waves Instruct the Wiring of the Visual Circuitry. Front Neural Circuits 10:54.

Bao ZZ (2008) Intraretinal projection of retinal ganglion cell axons as a model system for studying axon navigation. Brain Research 1192:165-177.

Bassett EA, Wallace VA (2012) Cell fate determination in the vertebrate retina. Trends in neurosciences 35:565-573.

Bastmeyer M, Ott H, Leppert CA, Stuermer CA (1995) Fish E587 glycoprotein, a member of the L1 family of cell adhesion molecules, participates in axonal fasciculation and the age-related order of ganglion cell axons in the goldfish retina. J Cell Biol 130:969-976.

Blank M, Koulen P, Blake DJ, Kroger S (1999) Dystrophin and beta-dystroglycan in photoreceptor terminals from normal and mdx3Cv mouse retinae. Eur J Neurosci 11:2121-2133.

Blankenship AG, Ford KJ, Johnson J, Seal RP, Edwards RH, Copenhagen DR, Feller MB (2009) Synaptic and extrasynaptic factors governing glutamatergic retinal waves. Neuron 62:230-241.

Booler HS, Williams JL, Hopkinson M, Brown SC (2016) Degree of Cajal-Retzius Cell Mislocalization Correlates with the Severity of Structural Brain Defects in Mouse Models of Dystroglycanopathy. Brain pathology (Zurich, Switzerland) 26:465-478.

Braunger BM, Demmer C, Tamm ER (2014) Programmed cell death during retinal development of the mouse eye. Adv Exp Med Biol 801:9-13.

Brittis PA, Lemmon V, Rutishauser U, Silver J (1995) Unique changes of ganglion cell growth cone behavior following cell adhesion molecule perturbations: a time-lapse study of the living retina. Mol Cell Neurosci 6:433-449.

Chai L, Morris JE (1999) Heparan sulfate in the inner limiting membrane of embryonic chicken retina binds basic fibroblast growth factor to promote axonal outgrowth. Exp Neurol 160:175-185.

Chan YM, Keramaris-Vrantsis E, Lidov HG, Norton JH, Zinchenko N, Gruber HE, Thresher R, Blake DJ, Ashar J, Rosenfeld J, Lu QL (2010) Fukutin-related protein is essential for mouse muscle, brain and eye development and mutation recapitulates the wide clinical spectrums of dystroglycanopathies. Hum Mol Genet 19:3995-4006.

Deiner MS, Kennedy TE, Fazeli A, Serafini T, Tessier-Lavigne M, Sretavan DW (1997) Netrin-1 and DCC mediate axon guidance locally at the optic disc: loss of function leads to optic nerve hypoplasia. Neuron 19:575-589.

Dobyns WB, Pagon RA, Armstrong D, Curry CJ, Greenberg F, Grix A, Holmes LB, Laxova R, Michels VV, Robinow M, et al. (1989) Diagnostic criteria for Walker-Warburg syndrome. Am J Med Genet 32:195-210.

Edwards MM, Mammadova-Bach E, Alpy F, Klein A, Hicks WL, Roux M, Simon-Assmann P, Smith RS, Orend G, Wu J, Peachey NS, Naggert JK, Lefebvre O, Nishina PM (2010) Mutations in Lama1 disrupt retinal vascular development and inner limiting membrane formation. J Biol Chem 285:7697-7711.

Ford KJ, Felix AL, Feller MB (2012) Cellular mechanisms underlying spatiotemporal features of cholinergic retinal waves. The Journal of neuroscience : the official journal of the Society for Neuroscience 32:850-863.

Fruh S, Romanos J, Panzanelli P, Burgisser D, Tyagarajan SK, Campbell KP, Santello M, Fritschy JM (2016) Neuronal Dystroglycan Is Necessary for Formation and Maintenance of Functional CCK-Positive Basket Cell Terminals on Pyramidal Cells. The Journal of neuroscience : the official journal of the Society for Neuroscience 36:10296-10313.

Fruttiger M (2007) Development of the retinal vasculature. Angiogenesis 10:77-88.
Fuerst PG, Koizumi A, Masland RH, Burgess RW (2008) Neurite arborization and mosaic spacing in the mouse retina require DSCAM. Nature 451:470-474.

Furuta Y, Lagutin O, Hogan BL, Oliver GC (2000) Retina- and ventral forebrain-specific Cre recombinase activity in transgenic mice. Genesis 26:130-132.

Galli-Resta L, Novelli E, Viegi A (2002) Dynamic microtubule-dependent interactions position homotypic neurones in regular monolayered arrays during retinal development. Development (Cambridge, England) 129:3803-3814.

Galli-Resta L, Resta G, Tan SS, Reese BE (1997) Mosaics of islet-1-expressing amacrine cells assembled by short-range cellular interactions. The Journal of neuroscience : the official journal of the Society for Neuroscience 17:7831-7838.

Gan L, Wang SW, Huang Z, Klein WH (1999) POU domain factor Brn-3b is essential for retinal ganglion cell differentiation and survival but not for initial cell fate specification. Developmental biology 210:469-480.

Gnanaguru G, Bachay G, Biswas S, Pinzon-Duarte G, Hunter DD, Brunken WJ (2013) Laminins containing the beta2 and gamma3 chains regulate astrocyte migration and angiogenesis in the retina. Development (Cambridge, England) 140:2050-2060.

Halfter W, Reckhaus W, Kroger S (1987) Nondirected axonal growth on basal lamina from avian embryonic neural retina. The Journal of neuroscience : the official journal of the Society for Neuroscience 7:3712-3722.

Halfter W, Willem M, Mayer U (2005) Basement membrane-dependent survival of retinal ganglion cells. Investigative ophthalmology & visual science 46:1000-1009.

Hayashi S, Lewis P, Pevny L, McMahon AP (2002) Efficient gene modulation in mouse epiblast using a Sox2Cre transgenic mouse strain. Mechanisms of development 119 Suppl 1:S97-s101.

Huckfeldt RM, Schubert T, Morgan JL, Godinho L, Di Cristo G, Huang ZJ, Wong ROL (2009) Transient neurites of retinal horizontal cells exhibit columnar tiling via homotypic interactions. Nature neuroscience 12:35-43.

Icha J, Kunath C, Rocha-Martins M, Norden C (2016) Independent modes of ganglion cell translocation ensure correct lamination of the zebrafish retina. J Cell Biol 215:259-275.

Kay JN, Chu MW, Sanes JR (2012) MEGF10 and MEGF11 mediate homotypic interactions required for mosaic spacing of retinal neurons. Nature 483:465-469.

Kay JN, Roeser T, Mumm JS, Godinho L, Mrejeru A, Wong ROL, Baier H (2004) Transient requirement for ganglion cells during assembly of retinal synaptic layers. Development (Cambridge, England) 131:1331-1342.

Lee Y, Kameya S, Cox GA, Hsu J, Hicks W, Maddatu TP, Smith RS, Naggert JK, Peachey NS, Nishina PM (2005) Ocular abnormalities in Large(myd) and Large(vls) mice, spontaneous models for muscle, eye, and brain diseases. Mol Cell Neurosci 30:160-172.

Li S, Sukeena JM, Simmons aB, Hansen EJ, Nuhn RE, Samuels IS, Fuerst PG (2015) DSCAM Promotes Refinement in the Mouse Retina through Cell Death and Restriction of Exploring Dendrites. Journal of Neuroscience 35:5640-5654.

Lunardi A, Cremisi F, Dente L (2006) Dystroglycan is required for proper retinal layering. Developmental biology 290:411-420.

Manzini MC, Gleason D, Chang BS, Hill RS, Barry BJ, Partlow JN, Poduri A, Currier S, Galvin-Parton P, Shapiro LR, Schmidt K, Davis JG, Basel-Vanagaite L, Seidahmed MZ, Salih MA, Dobyns WB, Walsh CA (2008) Ethnically diverse causes of Walker-Warburg syndrome (WWS): FCMD mutations are a more common cause of WWS outside of the Middle East. Human mutation 29:E231-241.

Marcos S, Nieto-Lopez F, Sandonìs A, Cardozo MJ, Marco FD, Esteve P, Bovolenta P (2015) Secreted Frizzled Related Proteins Modulate Pathfinding and Fasciculation of Mouse Retina Ganglion Cell Axons by Direct and Indirect Mechanisms. The Journal of neuroscience : the official journal of the Society for Neuroscience 35:4729-4740.

Montanaro F, Carbonetto S, Campbell KP, Lindenbaum M (1995) Dystroglycan expression in the wild type and mdx mouse neural retina: synaptic colocalization with dystrophin, dystrophin-related protein but not laminin. Journal of neuroscience research 42:528-538.

Moore CJ, Winder SJ (2010) Dystroglycan versatility in cell adhesion: a tale of multiple motifs. Cell communication and signaling : CCS 8:3.

Moore SA, Saito F, Chen J, Michele DE, Henry MD, Messing A, Cohn RD, Ross-Barta SE, Westra S, Williamson RA, Hoshi T, Campbell KP (2002) Deletion of brain dystroglycan recapitulates aspects of congenital muscular dystrophy. Nature 418:422-425.

Morgan J, Wong R (1995) Development of Cell Types and Synaptic Connections in the Retina. In: Webvision: The Organization of the Retina and Visual System (Kolb H, Fernandez E, Nelson R, eds). Salt Lake City (UT).

Myshrall TD, Moore SA, Ostendorf AP, Satz JS, Kowalczyk T, Nguyen H, Daza RA, Lau C, Campbell KP, Hevner RF (2012) Dystroglycan on radial glia end feet is required for pial basement membrane integrity and columnar organization of the developing cerebral cortex. J Neuropathol Exp Neurol 71:1047-1063.

Nakagawa N, Yagi H, Kato K, Takematsu H, Oka S (2015) Ectopic clustering of Cajal-Retzius and subplate cells is an initial pathological feature in Pomgnt2-knockout mice, a model of dystroglycanopathy. Scientific reports 5:11163.

Omori Y, Araki F, Chaya T, Kajimura N, Irie S, Terada K, Muranishi Y, Tsujii T, Ueno S, Koyasu T, Tamaki Y, Kondo M, Amano S, Furukawa T (2012) Presynaptic dystroglycan-pikachurin complex regulates the proper synaptic connection between retinal photoreceptor and bipolar cells. The Journal of neuroscience : the official journal of the Society for Neuroscience 32:6126-6137.

Ott H, Bastmeyer M, Stuermer CA (1998) Neurolin, the goldfish homolog of DM-GRASP, is involved in retinal axon pathfinding to the optic disk. The Journal of neuroscience : the official journal of the Society for Neuroscience 18:3363-3372.

Pan L, Deng M, Xie X, Gan L (2008) ISL1 and BRN3B co-regulate the differentiation of murine retinal ganglion cells. Development (Cambridge, England) 135:1981-1990.

Pinzon-Duarte G, Daly G, Li YN, Koch M, Brunken WJ (2010) Defective formation of the inner limiting membrane in laminin beta2- and gamma3-null mice produces retinal dysplasia. Investigative ophthalmology & visual science 51:1773-1782.

Randlett O, Poggi L, Zolessi FR, Harris Wa (2011) The oriented emergence of axons from retinal ganglion cells is directed by laminin contact in vivo. Neuron 70:266-280.

Reese BE (2011) Development of the retina and optic pathway. Vision research 51:613-632.

Reese BE, Necessary BD, Tam PP, Faulkner-Jones B, Tan SS (1999) Clonal expansion and cell dispersion in the developing mouse retina. Eur J Neurosci 11:2965-2978.

Riccomagno MM, Sun LO, Brady CM, Alexandropoulos K, Seo S, Kurokawa M, Kolodkin AL (2014) Cas adaptor proteins organize the retinal ganglion cell layer downstream of integrin signaling. Neuron 81:779-786.

Sato S, Omori Y, Katoh K, Kondo M, Kanagawa M, Miyata K, Funabiki K, Koyasu T, Kajimura N, Miyoshi T, Sawai H, Kobayashi K, Tani A, Toda T, Usukura J, Tano Y, Fujikado T, Furukawa T (2008) Pikachurin, a dystroglycan ligand, is essential for photoreceptor ribbon synapse formation. Nature neuroscience 11:923-931.

Satz JS, Barresi R, Durbeej M, Willer T, Turner A, Moore Sa, Campbell KP (2008) Brain and eye malformations resembling Walker-Warburg syndrome are recapitulated in mice by dystroglycan deletion in the epiblast. The Journal of neuroscience : the official journal of the Society for Neuroscience 28:10567-10575.

Satz JS, Ostendorf AP, Hou S, Turner A, Kusano H, Lee JC, Turk R, Nguyen H, Ross-Barta SE, Westra S, Hoshi T, Moore Sa, Campbell KP (2010) Distinct functions of glial and neuronal dystroglycan in the developing and adult mouse brain. The Journal of neuroscience : the official journal of the Society for Neuroscience 30:14560-14572.

Satz JS, Philp AR, Nguyen H, Kusano H, Lee J, Turk R, Riker MJ, Hernández J, Weiss RM, Anderson MG, Mullins RF, Moore SA, Stone EM, Campbell KP (2009) Visual impairment in the absence of dystroglycan. The Journal of neuroscience : the official journal of the Society for Neuroscience 29:13136-13146.

Takahashi H, Kanesaki H, Igarashi T, Kameya S, Yamaki K, Mizota A, Kudo A, Miyagoe-Suzuki Y, Takeda S, Takahashi H (2011) Reactive gliosis of astrocytes and Muller glial cells in retina of POMGnT1-deficient mice. Mol Cell Neurosci 47:119-130.

Takeda S, Kondo M, Sasaki J, Kurahashi H, Kano H, Arai K, Misaki K, Fukui T, Kobayashi K, Tachikawa M, Imamura M, Nakamura Y, Shimizu T, Murakami T, Sunada Y, Fujikado T, Matsumura K, Terashima T, Toda T (2003) Fukutin is required for maintenance of muscle integrity, cortical histiogenesis and normal eye development. Hum Mol Genet 12:1449-1459.

Taniguchi-Ikeda M, Morioka I, Iijima K, Toda T (2016) Mechanistic aspects of the formation of alpha-dystroglycan and therapeutic research for the treatment of alpha-dystroglycanopathy: A review. Mol Aspects Med 51:115-124.

Tao C, Zhang X (2016) Retinal Proteoglycans Act as Cellular Receptors for Basement Membrane Assembly to Control Astrocyte Migration and Angiogenesis. Cell Rep 17:1832-1844.

Taylor L, Arner K, Engelsberg K, Ghosh F (2015) Scaffolding the retina: the interstitial extracellular matrix during rat retinal development. Int J Dev Neurosci 42:46-58.

Thompson H, Camand O, Barker D, Erskine L (2006) Slit proteins regulate distinct aspects of retinal ganglion cell axon guidance within dorsal and ventral retina. The Journal of neuroscience : the official journal of the Society for Neuroscience 26:8082-8091.

Tronche F, Kellendonk C, Kretz O, Gass P, Anlag K, Orban PC, Bock R, Klein R, Schutz G (1999) Disruption of the glucocorticoid receptor gene in the nervous system results in reduced anxiety. Nat Genet 23:99-103.

Varshney S, Hunter DD, Brunken WJ (2015) Extracellular Matrix Components Regulate Cellular Polarity and Tissue Structure in the Developing and Mature Retina. J Ophthalmic Vis Res 10:329-339.

Wang SW, Kim BS, Ding K, Wang H, Sun D, Johnson RL, Klein WH, Gan L (2001) Requirement for math5 in the development of retinal ganglion cells. Genes Dev 15:24-29.

Wassle H, Riemann HJ (1978) The mosaic of nerve cells in the mammalian retina. Proc R Soc Lond B Biol Sci 200:441-461.

Wright KM, Lyon KA, Leung H, Leahy DJ, Ma L, Ginty DD (2012) Dystroglycan organizes axon guidance cue localization and axonal pathfinding. Neuron 76:931-944.

Xiao T, Staub W, Robles E, Gosse NJ, Cole GJ, Baier H (2011) Assembly of lamina-specific neuronal connections by slit bound to type IV collagen. Cell 146:164-176.

Xu HP, Burbridge TJ, Ye M, Chen M, Ge X, Zhou ZJ, Crair MC (2016) Retinal Wave Patterns Are Governed by Mutual Excitation among Starburst Amacrine Cells and Drive the Refinement and Maintenance of Visual Circuits. The Journal of neuroscience : the official journal of the Society for Neuroscience 36:3871-3886.

Yang L, Cai CL, Lin L, Qyang Y, Chung C, Monteiro RM, Mummery CL, Fishman GI, Cogen A, Evans S (2006) Isl1Cre reveals a common Bmp pathway in heart and limb development. Development (Cambridge, England) 133:1575-1585.

Young RW (1984) Cell death during differentiation of the retina in the mouse. J Comp Neurol 229:362-373.

Yurchenco PD (2011) Basement membranes: cell scaffoldings and signaling platforms. Cold Spring Harb Perspect Biol 3.

Figure Legends

Figure 1: The inner limiting membrane undergoes progressive degeneration in the absence of functional dystroglycan. (A) Dystroglycan (β-DG) is expressed throughout the developing retina, with an enrichment at the inner limiting membrane (ILM). (B) Dystroglycan expression is lost in *DG$^{F/-}$; Sox2^{Cre}* mice. (C-E) The initial assembly of the ILM (laminin, green) occurs normally in the absence of functional dystroglycan in (D) *ISPD$^{L79*/L79*}$* and (E) *DG$^{F/-}$; Sox2^{cre}* retinas. The ILM in *ISPD$^{L79*/L79*}$* and *DG$^{F/-}$; Sox2^{cre}* retinas undergoes progressive degeneration at e16 (middle) and P0 (right), and retinal neurons migrate into the vitreous. (F) The ILM in *ISPD$^{L79*/L79*}$* retinas undergoes degeneration (right panel) that is present across the entire span of the retina at e16. Arrowheads indicate ILM, asterisks indicate non-specific staining of blood vessels. Scale bar, 50μm A-D, 200 μm E.

Figure 2: Dystroglycan is required to localize ECM proteins at the ILM. (A) Multiple extracellular matrix proteins, including laminin (purple), collagen IV (red), and perlecan (green), localize to the ILM in controls. (B-**C**) Localization of extracellular matrix proteins is disrupted in the ILM in the absence of functional dystroglycan in *ISPD$^{L79*/L79*}$* (B) and *DG$^{F/-}$; Sox2^{cre}* (C) retinas at P0. Arrowheads indicate ILM, asterisks indicate blood vessels. Scale bar, 50μm.

Figure 3: Dystroglycan regulates normal retinal vasculature development. (A) IB4 labeled hyaloid vasculature is present in the vitreous adjacent to the GCL in control retinas (left) but is embedded within ectopic cell clusters *ISPD$^{L79*/L79*}$* (right) retinas at e16. (B) Flat mount retinas at P0 show the emergence of the primary vascular plexus (IB4, green) and astrocytes (GFAP, purple) in controls (left). In *ISPD$^{L79*/L79*}$* retinas (right), the emergence of astrocytes and the primary vascular plexus into the retina is delayed (arrow) and there is a persistence of hyaloid vasculature. Scale bar 50 μm A, 100 μm B.

Figure 4: Dystroglycan is required for intraretinal axon guidance, (A) L1 positive axons in the optic fiber layer (OFL) initially appear normal in *ISPD$^{L79*/L79*}$* (middle), and *DG$^{F/-}$; Sox2^{cre}* retinas (right) at e13. (B, C) As the ILM degenerates in *ISPD$^{L79*/L79*}$* and *DG$^{F/-}$; Sox2^{cre}* retinas at e16 (B) and P0 (C), axons hyperfasciculate (arrowhead) and exhibit defasciculation (asterisk) within the OFL. (D, E). Flat mount preparations from *ISPD$^{L79*/L79*}$* and *DG$^{F/-}$; Sox2^{cre}* retinas at e16 (D) and P0 (E) show progressive disruption of axon tracts (Neurofilament, 2H3). Scale bar, 50 μm.

Figure 5: Conditional deletion of *dystroglycan* in the developing retina results in migration and axon guidance defects. (A) Recombination pattern of *Rosa26-lox-stop-lox-TdTomato; Ai9* reporter (green) by *Six3^{cre}* shows expression throughout the retina and in axons at e13. (B) Dystroglycan protein expression is lost in *DG$^{F/-}$; Six3^{cre}* mice. (C, D) *DG$^{F/-}$; Six3^{cre}* (right) mice exhibit inner limiting membrane degeneration (top, purple, laminin) and abnormal axonal fasciculation and guidance (top, green, bottom, 2H3). (E) Primary vascular plexus (IB4, green) and astrocytes (GFAP, purple) migrate from the optic nerve head (dashed circle) to the edge of the retina (dashed line) in

control retinas at P14 (right). Vascular and astrocyte migration is stunted in *DG*$^{F/-}$; *Six3*^{cre} retinas. (F) Focal migration defects (arrowheads) in P7 *DG*$^{F/-}$; *Six3*^{cre} retinas are present across the entire span of the retina. Green arrowhead indicates high magnification image in F (right). Scale bar 100 μm A left, 500 μm F left**,** E, 50 μm A, D right, B-D.

Figure 6: Disrupted postnatal circuit formation in the inner retina of *dystroglycan* mutants. (A) Photoreceptors (recoverin) have normal lamination in P14 *DG*$^{F/-}$; *Six3*^{cre} retinas (right). (B-C) The cell bodies of bipolar cells (PKC, B, SCGN, C) exhibit normal lamination patters, while their axons extend into ectopic cellular clusters in the ganglion cell layer. (D-G) Abnormal cellular lamination and disruptions in dendritic stratification of multiple amacrine and retinal ganglion cell types is observed in *DG*$^{F/-}$; *Six3*^{cre} retinas. (D) ChAT labels starburst amacrine cells, (E) calbindin and (F) calretinin label amacrine and ganglion cells, and (G) GlyT1 labels glycinergic amacrine cells. (H) Müller glia (glutamine synthetase) cell bodies are normally positioned while their inner retinal processes extend into ectopic cellular clusters. Arrowheads indicate axons or cell bodies in ectopic clusters, arrows indicate horizontal cell layer. Scale bar, 50 μm.

Figure 7: Dystroglycan is required for mosaic cell spacing in the ganglion cell layer. (A, B). Horizontal cells (2H3) in flat mount P14 adult retinas have reduced cellular density, but normal mosaic cell spacing curves (Nearest neighbor analysis, $p<0.0001$, Two-Way ANOVA, Tukey HSD post-hoc test ***$p<0.0001$, n=20 samples from 5 control retinas, 18 samples from 5 mutant retinas). (C, D) Mosaic cell spacing of starburst amacrine cells (ChAT) in the inner nuclear layer is normal (Nearest neighbor analysis, Two-Way ANOVA, Tukey HSD post-hoc test *$p=0.0494$, n=10 samples from 3 control retinas, 10 samples from 3 mutant retinas), while the ectopic clustering of starburst amacrine cells in the ganglion cell layer results in a significant disruption of mosaic spacing (Nearest neighbor analysis, $p<0.0001$, Two-Way ANOVA, Tukey HSD post-hoc test ***$p<0.0001$, n=10 samples from 3 control retinas, 10 samples from 3 mutant retinas). Scale bar 100μm.

Figure 8: Retinal thinning in *dystroglycan* mutants. (A-D) P14 *DG*$^{F/-}$; *Six3*^{cre} retinas show decreased retinal thickness (DAPI, $p=0.0039$, t test, n=7 control, 7 mutant), a decreased thickness of the photoreceptor layer (C, Recoverin, green, $p=0.0163$, t-test, n=7 control, 7 mutant) and no change in thickness of the bipolar cell layer (D, Chx10, purple, $p>0.05$, t-test, n=7 control, 7 mutant). Starburst amacrine cell density is normal in both the INL (E, $p>0.05$, t-test, n=10 samples from 3 control retinas, 10 samples from 3 mutant retinas)and GCL (F, $p>0.05$, t-test, n=10 samples from 3 control retinas, 10 samples from 3 mutant retinas), while horizontal cells show a slight reduction in cell density (G) in P14 *DG*$^{F/-}$; *Six3*^{cre} retinas ($p=0.0112$, t test, n=20 samples from 5 control retinas, 18 samples from 5 mutant retinas). (H, I) Ganglion cell density (RBPMS) is reduced by approximately 50% in P14 *DG*$^{F/-}$; *Six3*^{cre} retinas ($p<0.0001$, t-test, n=12 samples from 3 control retinas, 12 samples from 3 mutant retinas). Scale bar 50 μm.

Figure 9: Loss of dystroglycan results in increased developmental cell death. (A) Immunohistochemistry for mitotic cells (PH3) at e13 (top) and e16 (bottom) shows

normally positioned mitotic retinal progenitor cells adjacent to the RPE. (B) Quantification of mitotic cells shows no difference between control and ISPD$^{L79*/L79*}$ -mutants (p>0.05, t test, n=4 control and 4 mutant retinas at e13, p>0.05, t test, n=4 control and 4 mutant retinas at e16). (C-D) Immunohistochemistry for cleaved caspase-3 in a flat mount preparation of P0 *DG$^{F/-}$; Six3^{cre}* retinas shows an increase in apoptotic cells. (p=0.0279, t test, n=18 samples from 6 control retinas, 17 samples from 6 mutant retinas). (D) Quantification of cleaved caspase-3 positive cells shows an increase in apoptotic cells at e16 (p<0.0001, t test, n=18 samples from 6 control retinas, 18 samples from 8 mutant retinas) and P0 (C, D p<0.0001, t test, n=18 samples from 6 control retinas, 15 samples from 5 mutant retinas) between control (left) and *ISPD$^{L79*/L79*}$* (middle) retinas. Scale bar 50 μm.

Figure 10: Dystroglycan is not required within RGCs for their migration and axon outgrowth. (A) Recombination pattern of *Rosa26-lox-stop-lox-TdTomato; Ai9* reporter (green) by *Isl1^{cre}* by shows expression the majority of differentiated ganglion cells at e12.5 (left) and P0 (right). (B) Dystroglycan expression at the ILM is unchanged between control and *DG$^{F/-}$; Isl1^{cre}* retinas. (C) The ILM (laminin, purple) and axons in the OFL (2H3, green) in *DG$^{F/-}$; Isl1^{cre}* retinas appear similar to control. (D) Flat mount preparations show normal axon fasciculation (2H3) in *DG$^{F/-}$; Isl1^{cre}* retinas. (E-F) *DG$^{F/-}$; Isl1^{cre}* (right panel) retinas (P14) have normal cellular lamination and dendritic stratification. Dashed line indicates ILM. Asterisk notes a differentiated ganglion cell body that is still migrating toward the ILM. Scale bar 20 μm A left panel, scale bar 50 μm A right panel, B-**F**.

Figure 11: The intracellular signaling domain of dystroglycan is not required for proper retinal development. (A) ILM integrity (laminin, purple), neuronal migration (DAPI, blue) and axon outgrowth (2H3, green) all appear normal in mice lacking the intracellular domain of dystroglycan (*DG$^{-/-}_{\beta}$cyt*) at P0. (B) Flat mount preparations show normal axon fasciculation (2H3) in *DG$^{-/-}_{\beta}$cyt* retinas. (C-D) *DG$^{-/-}_{\beta}$cyt* retinas (P28) have normal cellular lamination and dendritic stratification. Scale bar, 50 μm.

Figure 12: Synaptic markers are present in the retina of *dystroglycan* mutants. (A) Markers for outer retinal ribbon synapses (Ribeye, presynaptic and mGluR6, postsynaptic) appear structurally normal in the absence of dystroglycan. The density of (B) excitatory (VGLUT1) and (C) inhibitory (VGAT) presynaptic markers appear similar to control in the inner retinas of *DG$^{F/-}$; Six3^{cre}* mutants. Synapses are also present within ectopic clusters (asterisks). Scale bar, 50 μm wide view, scale bar,10 μm enlarged view.

Figure 13: Dystroglycan is dispensable for the generation and propagation of retinal waves. (A-B) At P1, waves propagate normally across the retina in *DG$^{F/+}$; Six3^{cre}; R26-LSL-GCaMP6f* (A) and *DG^{F-}; Six3^{cre}; R26-LSL-GCaMP6f* mice (B). (C) Distributions of wave areas show no difference between controls and mutants (Wilcoxon rank sum test, p>0.05). (D) Wave propagation rate is slightly slower in mutant retinas (Wilcoxon rank sum test, p=0.0493). Wave parameters were calculated from 142 control waves obtained from 6 retinas from 3 control mice and 173 mutant waves obtained from

8 retinas from 5 mutant mice. Arrowheads indicate the initiation site of a retinal wave. Scale bar 500 μm. Time displayed in milliseconds.

Table 1: List of Antibodies. Antibodies utilized throughout the study, including target, host species, dilution, manufacturer, catalog number and RRID.

Movie 1: Retinal waves in *DG*$^{F/+}$*; Six3*^{cre}*; R26-LSL-GCaMP6f* mice. 15frames/sec, total of 21 frames

Movie 2: Retinal waves in *DG*$^{F/-}$*; Six3*^{cre}*; R26-LSL-GCaMP6f* mice. 15frames/sec, total of 21 frames

Figure 1

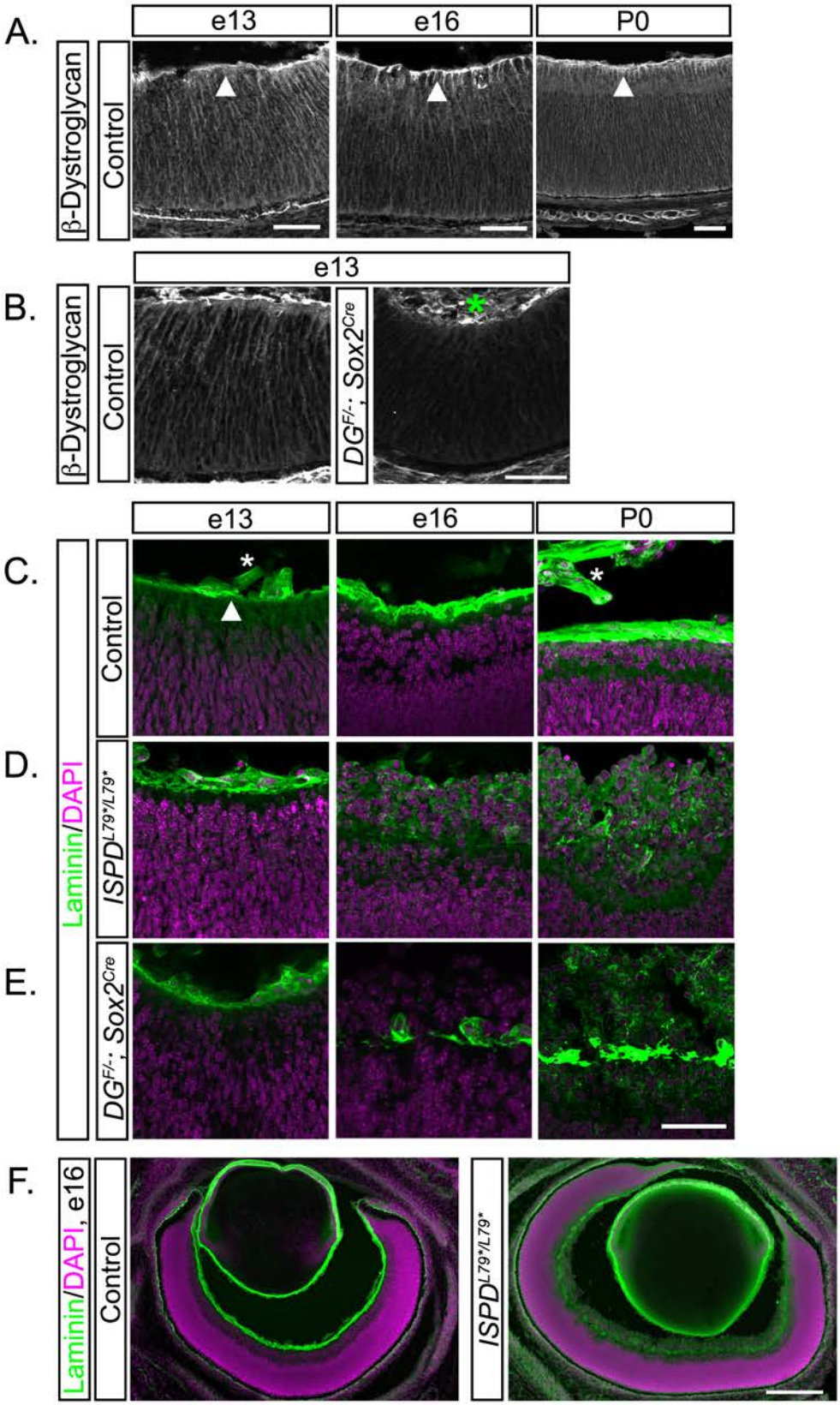
A.
e13
e16
P0
β-Dystroglycan
Control
B.
e13
β-Dystroglycan
Control
DG^F/-; Sox2^Cre
C.
e13
e16
P0
Control
D.
ISPD^L79*/L79*
E.
DG^F/-; Sox2^Cre
Laminin/DAPI
F.
Laminin/DAPI, e16
Control
ISPD^L79*/L79*

Figure 2

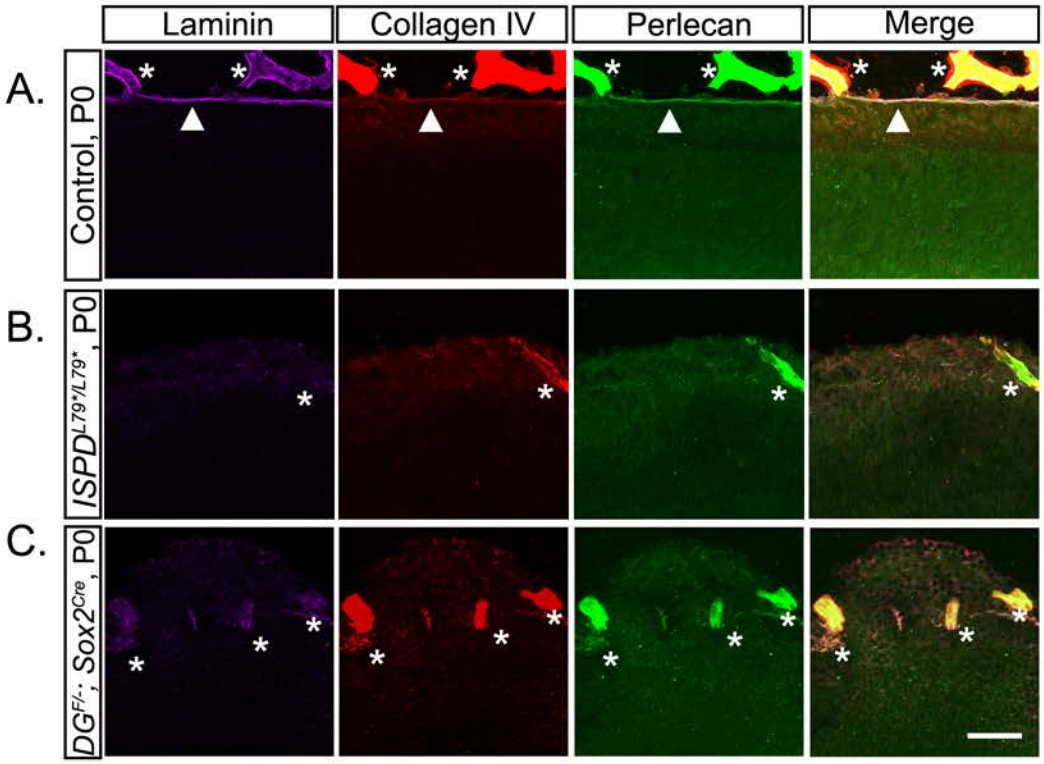
Laminin
Collagen IV
Perlecan
Merge
A.
Control, P0
B.
ISPD L79*/L79*, P0
C.
DGF/-*; Sox2Cre, P0

Figure 3

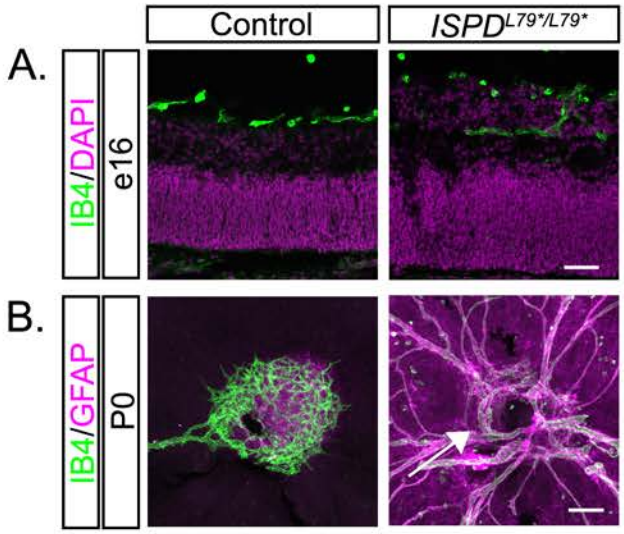

Figure 4

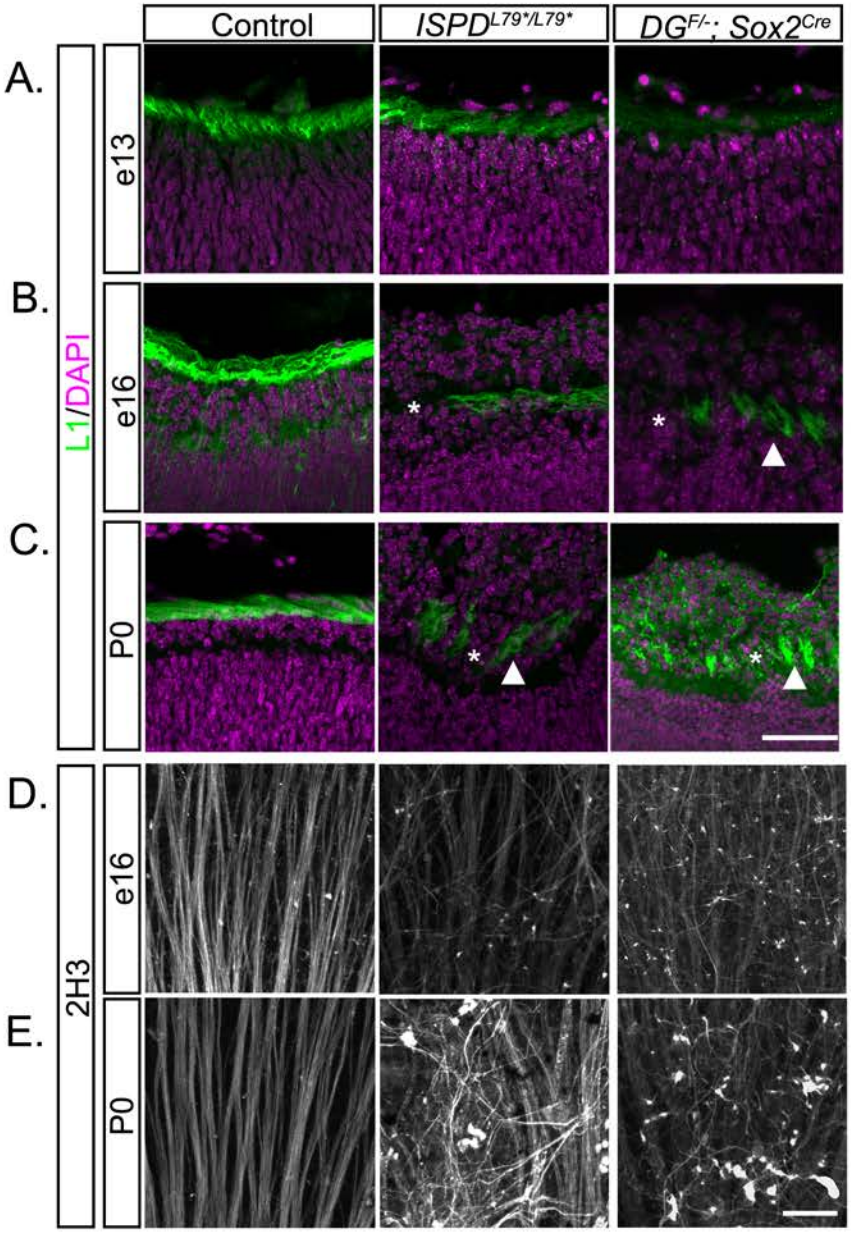
Control
ISPD L79*/L79*
DG F/-; Sox2 Cre
A.
B.
C.
D.
E.
L1/DAPI
2H3
e13
e16
P0
e16
P0

Figure 5

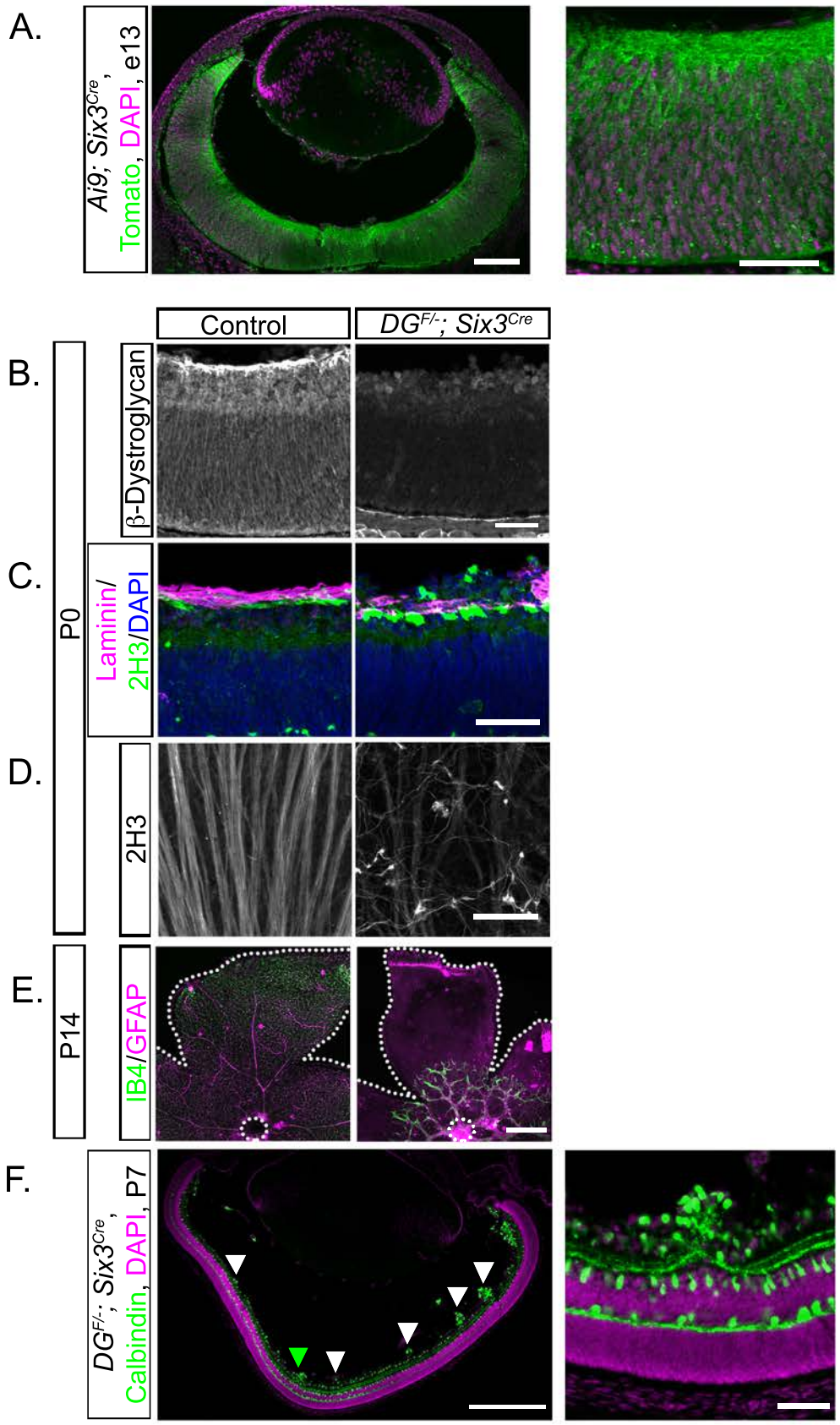
A.
Ai9; Six3Cre,
Tomato, DAPI, e13
Control
DGF/-; Six3Cre
B.
β-Dystroglycan
C.
Laminin/
2H3/DAPI
D.
2H3
P0
E.
IB4/GFAP
P14
F.
DGF/-; Six3Cre,
Calbindin, DAPI, P7

Figure 6

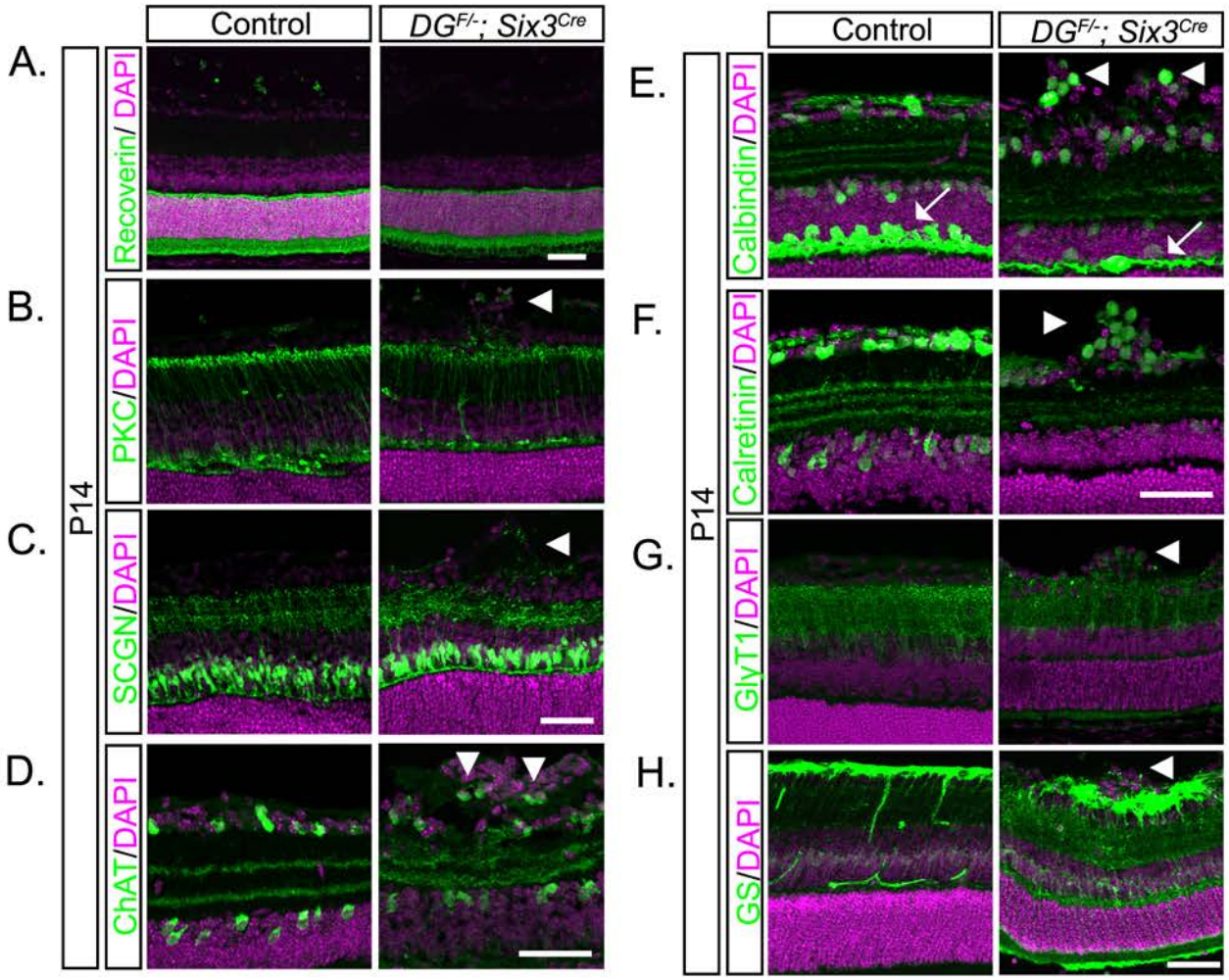
Control
DG$^{F/-}$; Six3^{Cre}
A.
B.
C.
D.
P14
Recoverin/ DAPI
PKC/DAPI
SCGN/DAPI
ChAT/DAPI
E.
F.
G.
H.
Calbindin/DAPI
Calretinin/DAPI
GlyT1/DAPI
GS/DAPI

Figure 7

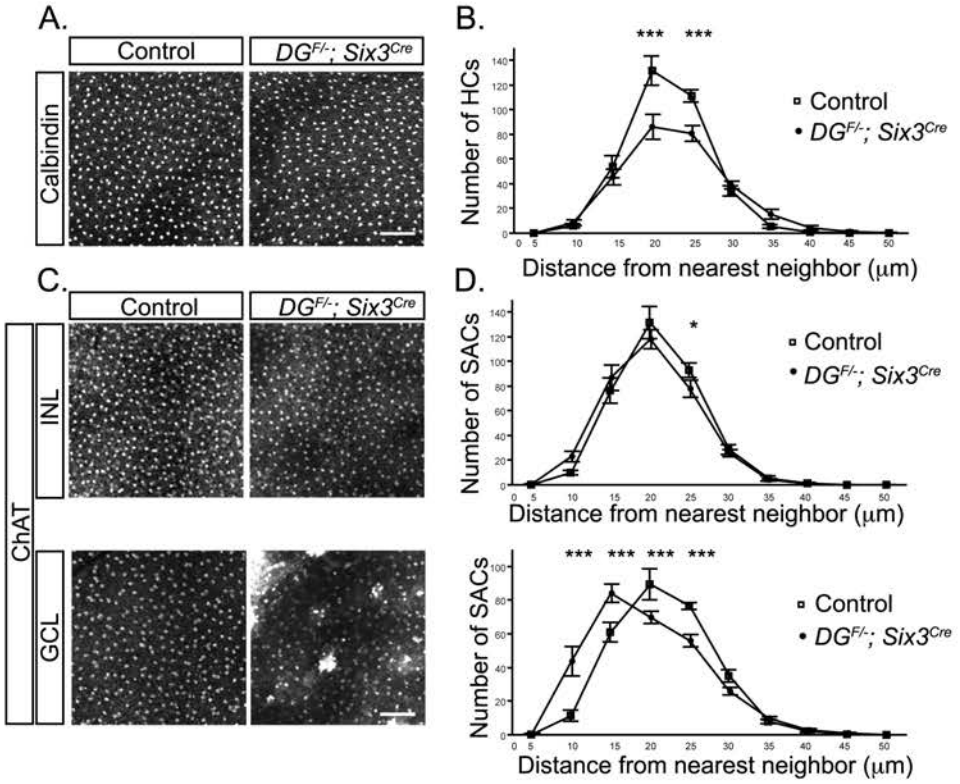
A.
Control
DG$^{F/-}$; Six3^{Cre}
Calbindin
B.
***
***
Number of HCs
Control
DG$^{F/-}$; Six3^{Cre}
Distance from nearest neighbor (μm)
C.
Control
DG$^{F/-}$; Six3^{Cre}
ChAT
INL
GCL
D.
*
Number of SACs
Control
DG$^{F/-}$; Six3^{Cre}
Distance from nearest neighbor (μm)
***
***
***
***
Number of SACs
Control
DG$^{F/-}$; Six3^{Cre}
Distance from nearest neighbor (μm)

Figure 8

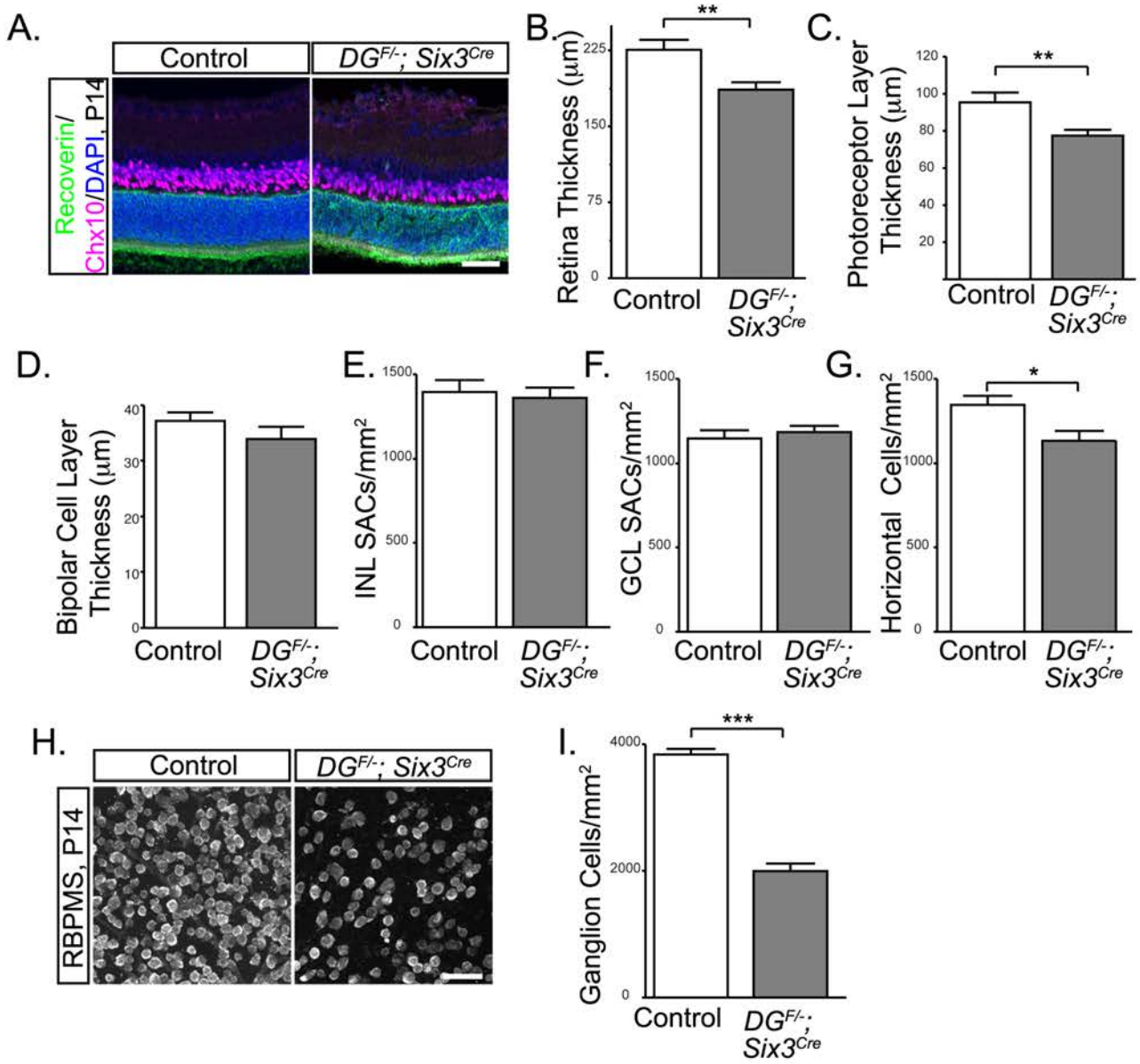
A.
Control
DG$^{F/-}$; Six3^{Cre}
Recoverin/
Chx10/DAPI, P14
B.
Retina Thickness (μm)
225
150
75
0
**
Control
DG$^{F/-}$; Six3^{Cre}
C.
Photoreceptor Layer Thickness (μm)
120
100
80
60
40
20
**
Control
DG$^{F/-}$; Six3^{Cre}
D.
Bipolar Cell Layer Thickness (μm)
40
30
20
10
0
Control
DG$^{F/-}$; Six3^{Cre}
E.
INL SACs/mm^2
1500
1000
500
0
Control
DG$^{F/-}$; Six3^{Cre}
F.
GCL SACs/mm^2
1500
1000
500
0
Control
DG$^{F/-}$; Six3^{Cre}
G.
Horizontal Cells/mm^2
1500
1000
500
0
*
Control
DG$^{F/-}$; Six3^{Cre}
H.
Control
DG$^{F/-}$; Six3^{Cre}
RBPMS, P14
I.
Ganglion Cells/mm^2
4000
2000
0
***
Control
DG$^{F/-}$; Six3^{Cre}

Figure 9

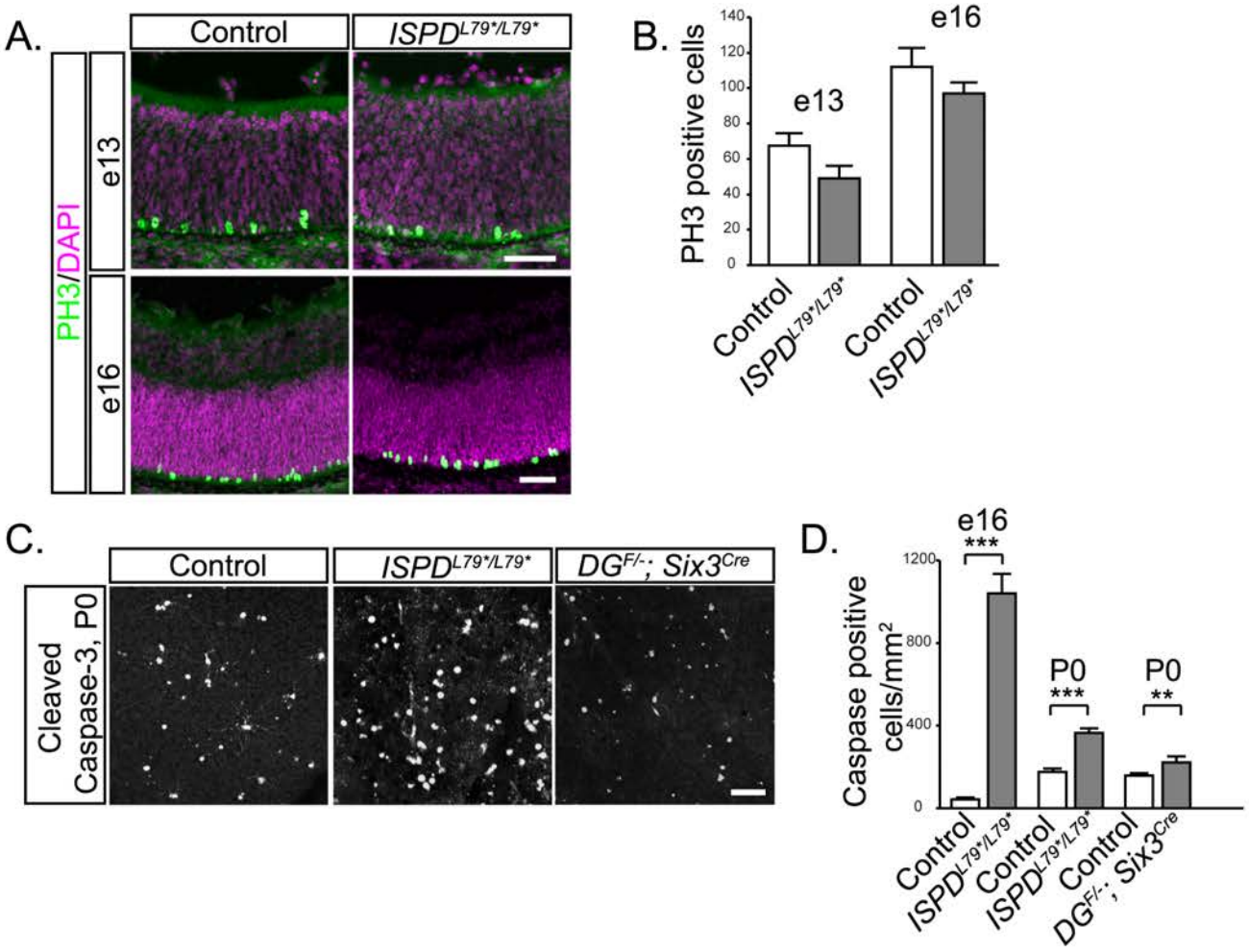
A.
Control
ISPD L79*/L79*
PH3/DAPI
e13
e16
B.
PH3 positive cells
e13
e16
140
120
100
80
60
40
20
0
Control
ISPD L79*/L79*
Control
ISPD L79*/L79*
C.
Control
ISPD L79*/L79*
DG F/-; Six3 Cre
Cleaved Caspase-3, P0
D.
Caspase positive cells/mm2
e16
***
P0
***
P0
**
1200
800
400
0
Control
ISPD L79*/L79*
Control
ISPD L79*/L79*
Control
DG F/-; Six3 Cre

Figure 10

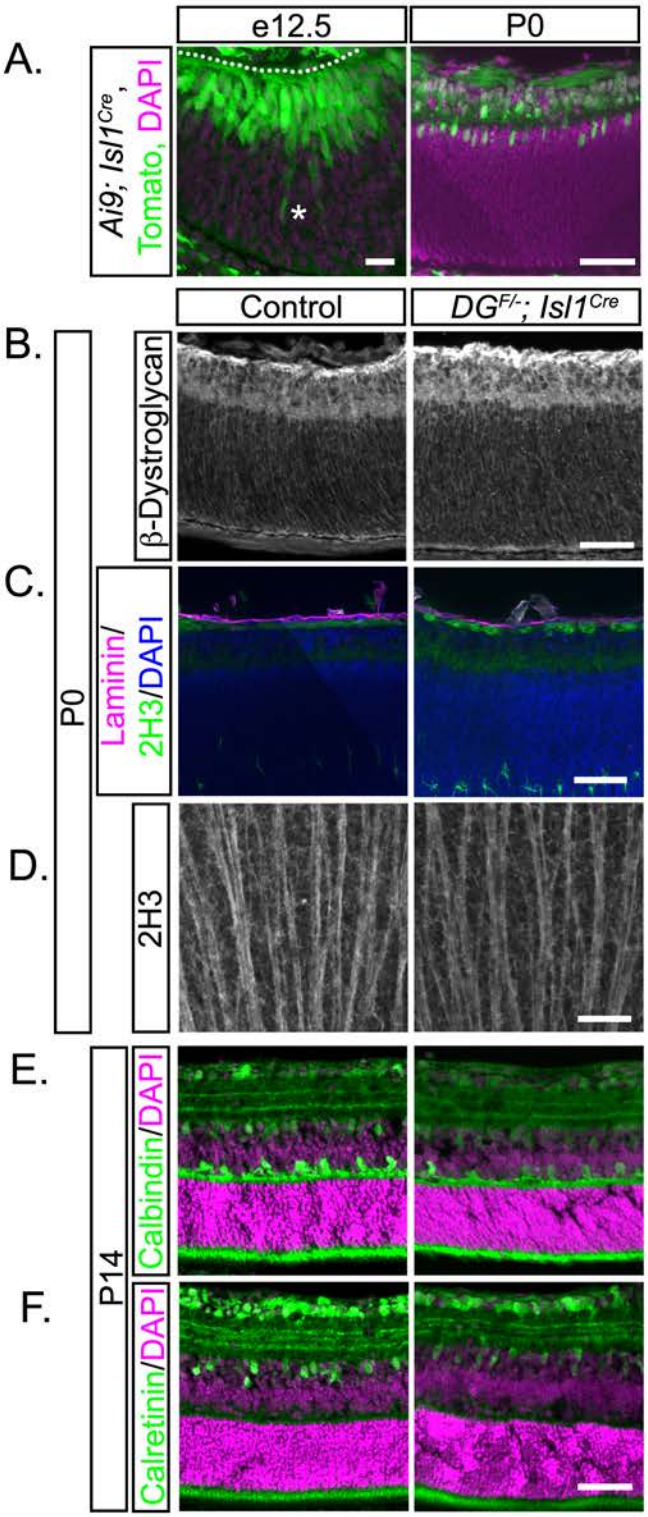
A.
e12.5
P0
Ai9; Isl1Cre,
Tomato, DAPI
*
B.
Control
DGF/-; Isl1Cre
P0
β-Dystroglycan
C.
Laminin/
2H3/DAPI
D.
2H3
E.
P14
Calbindin/DAPI
F.
Calretinin/DAPI

Figure 11

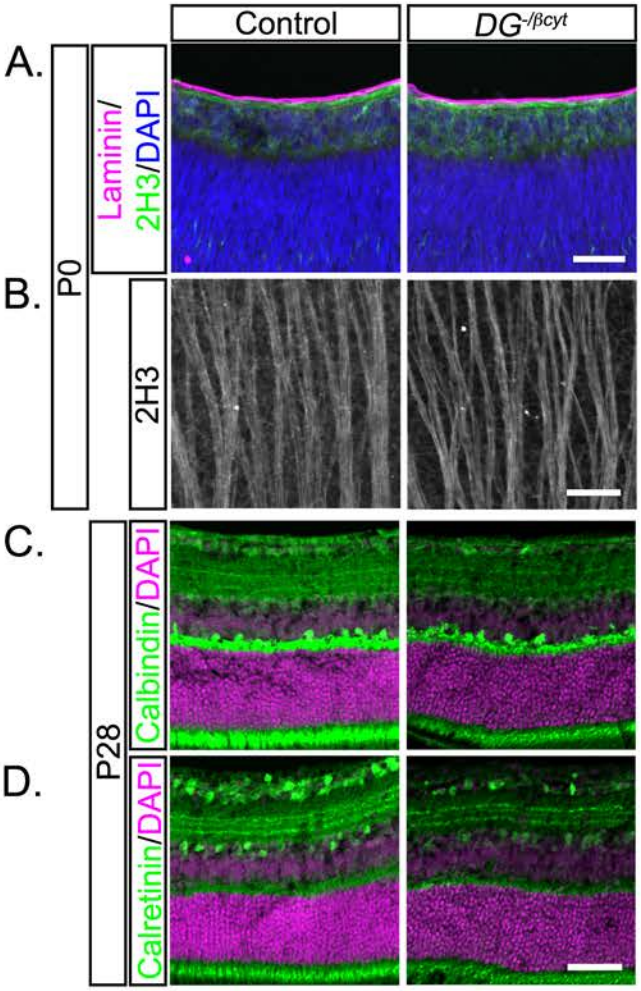
Control
DG-/βcyt
A.
B.
C.
D.
P0
P28
Laminin/
2H3/DAPI
2H3
Calbindin/DAPI
Calretinin/DAPI

Figure 12

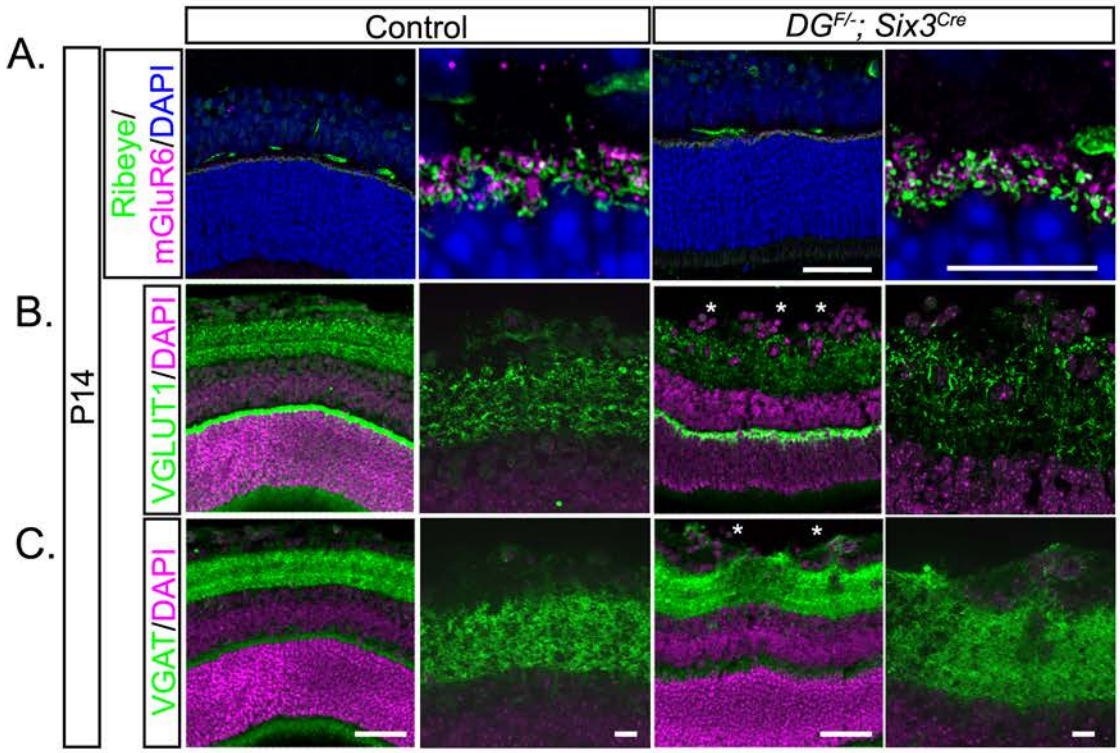
Control
DG$^{F/-}$; Six3^{Cre}
A.
B.
C.
P14
Ribeye/
mGluR6/DAPI
VGLUT1/DAPI
VGAT/DAPI

Figure 13

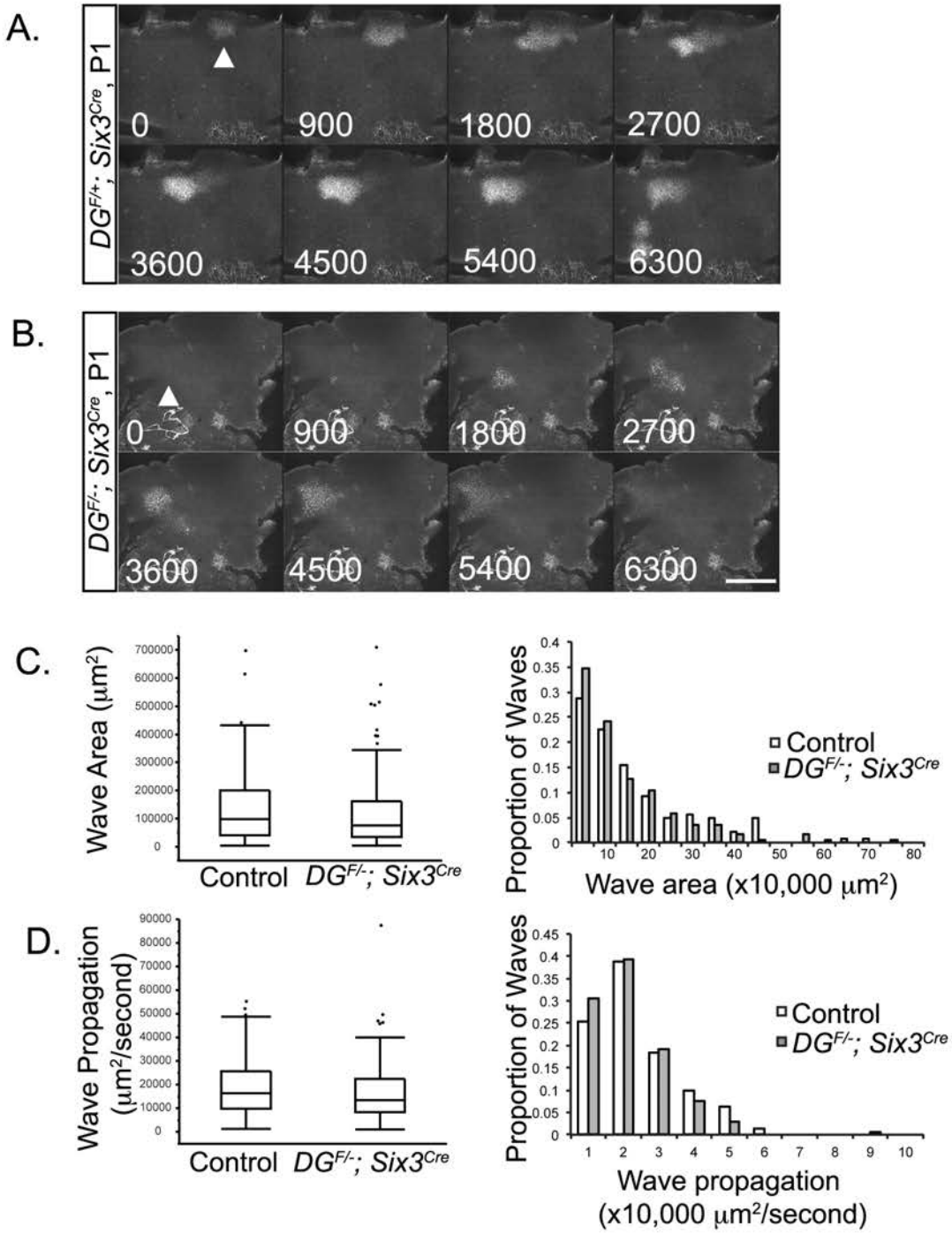
A.
DG^F/+; Six3^Cre, P1
0
900
1800
2700
3600
4500
5400
6300
B.
DG^F/-; Six3^Cre, P1
0
900
1800
2700
3600
4500
5400
6300
C.
Wave Area (μm²)
Control
DG^F/-; Six3^Cre
Proportion of Waves
Control
DG^F/-; Six3^Cre
Wave area (x10,000 μm²)
D.
Wave Propagation (μm²/second)
Control
DG^F/-; Six3^Cre
Proportion of Waves
Control
DG^F/-; Six3^Cre
Wave propagation (x10,000 μm²/second)

Table 1: Antibodies

Target	Host species	Dilution	Company/origin	Catalog #	RRID
2H3	mouse	1:1000	DSHB	2h3	AB_531793
β-Dystroglycan	mouse	1:500	DSHB	MANDAG2(7D11)	AB_2618140
β-Dystroglycan	rabbit	1:100	Santa Cruz Biotech	sc-28535	AB_782259
Calbindin	rabbit	1:10,000	Swant	CB 38	AB_10000340
Calretinin	rabbit	1:10,000	Swant	CG 1	AB_2619710
ChAT	goat	1:500	Millipore	AB144P-200UL	AB_11214092
Chx10	goat	1:500	Santa Cruz Biotech	sc-21690	AB_2216006
Cleaved Caspase-3	rabbit	1:500	Cell Signaling	9661S	AB_2341188
Collagen IV	goat	1:250	Southern Biotech	1340-01	AB_2082646
Glutamine Synthetase	mouse	1:1000	BD Biosciences	610517	AB_397879
GlyT1	rabbit	1:800	gift from Dr. David Pow		
IB4		1:250	Life Technologies	I21411	AB_2314662
L1	rat	1:500	Millipore	MAB5272	AB_2133200
Laminin	rabbit	1:1000	Sigma	L9393	AB_477163

MGluR6	sheep	1:100	gift from Dr. Catherine Morgans		
Perlecan	rat	1:500	Millipore	MAB1948P	AB_10615958
PKC	mouse	1:500	Sigma	P5704	AB_477375
RBPMS	guinea pig	1:500	PhosphoSolutions	1832-RBPMS	AB_2492226
Recoverin	rabbit	1:200	Millipore	AB5585	AB_2253622
Ribeye/Ctbp2	mouse	1:1000	BD Biosciences	612044	AB_399431
Secretagogin	rabbit	1:4000	Biovendor	rd181120100	AB_2034060
VGAT	rabbit	1:500	Synaptic Systems	131-003	AB_887869
VGLUT1	guinea pig	1:500	Millipore	AB5905	AB_2301751